

**An-Najah National University  
Faculty of Graduate Studies**

**Effects of a Uniform Applied Magnetic Field and  
Temperature on the Magnetic Properties of the Dipolar Anti-  
ferromagnetic planar System: Parametric Study**

**By**

**Naim "Ahmed Rasheed" Mahmoud Malak**

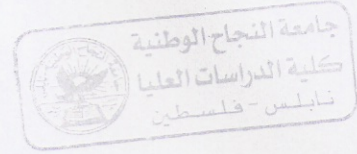
**Supervised by**

**Dr. Abdel-Rahman Mustafa Abu-Labdeh**

*submitted in Partial Fulfillment of the Requirements for the Degree of  
Master of Science in Physics, Faculty of Graduate Studies, at AN-Najah  
National University, Nablus, Palestine.*

**2008**

Abdel-Rahman



**Effects of a Uniform Applied Magnetic Field and Temperature on the  
Magnetic Properties of the Dipolar Anti-ferromagnetic Planar System:  
Parametric Study**

by

**Naim "Ahmed Rasheed" Mahmoud Malak**

*This Thesis was defended successfully on 27/08/2008 and approved by*

**Committee Members**

- 1- **Dr. Abdel – Rahman M. A. Labdeh (Supervisor)**  
Assistant Professor of Physics
- 2- **Prof. Dr. Imad Barghouthi (External Examiner)**  
Professor of Physics
- 3- **Dr. Mohammed S. Abu Jafar (Internal Examiner)**  
Associate Professor of Physics

**Signature**

Abdel-Rahman

Imad Barghouthi

Mohammed S. Abu Jafar

## **Dedication**

*To the Memory of my Father*

*"God Mercify him"*

## Acknowledgements

I would like to express my gratitude and deepest appreciation to Dr. Abdel-Rahman Mustafa Abu-Labdeh for his guidance, encouragement, and great efforts. That is; without his help, this work would never have been done.

I'd like to appreciate the efforts of the committee members represented by Prof. Dr. Imad A. Barghouthi (*Al-Quds University*) as an external examiner, and Dr. Mohammed S. Abu-Jafar (*Dean of Graduate Studies - An-Najah National University*) as an internal examiner.

I thank the Physics Department at An-Najah National University headed by Dr. Mousa El-Hasan and all instructors who stand behind the Master's Program in physics. I will never forget the favor and efforts of Prof. Dr. Issam Rashid, Dr. Mohammed S. Abu-Jafar, Dr. Abdel-Rahman Mustafa Abu-Labdeh, Prof. Dr. Sami Jabbir, and Dr. Salman Salman.

Special thanks to my friends Omar, Farah, Naser, Thaer, Kamal, and all my classmates in the program.

Finally, this work was supported in part by the Natural Sciences and Engineering Research Council of Canada. I gratefully acknowledge access to Computational Resources through Western Canada Research Grid *WestGrid* and Shared Hierarchical Academic Research Computing Network *SHARCNET*.

## إقرار

أنا الموقع أدناه مقدم الرسالة التي تحمل العنوان:

### **Effects of a Uniform Applied Magnetic Field and Temperature on the Magnetic Properties of the Dipolar Anti-ferromagnetic planar System: Parametric Study**

أقر بأن ما اشتملت عليه هذه الرسالة، إنما هي نتاج جهدي الخاص، باستثناء ما تمت الإشارة إليه حيثما ورد، وأن هذه الرسالة ككل، أو أي جزء منها لم يقدم من قبل لنيل أية درجة علمية أو بحث علمي أو بحثي لدى أية مؤسسة تعليمية أو بحثية أخرى.

## Declaration

The work provided in this thesis, unless otherwise referenced, is the researchers own work, and has not been submitted elsewhere for any other degree or qualification.

**Student's name:**

**اسم الطالب:**

**Signature:**

**التوقيع:**

**Date:**

**التاريخ:**

## Table of Contents

<b>Subject</b>	<b>page</b>
Dedication	<b>iii</b>
Acknowledgements	<b>iv</b>
Declaration	<b>v</b>
Table of Contents	<b>vi</b>
List of Figures	<b>vii</b>
Abstract	<b>ix</b>
1 Introduction	<b>1</b>
2 The Model in General Terms	<b>12</b>
3 Monte Carlo Simulations and the Computational Details	<b>18</b>
3.1 Importance Sampling, Detailed Balance, and Metropolis Algorithm	<b>19</b>
3.2 Computational Aspects	<b>25</b>
4 Results and Discussion	<b>29</b>
4.1 Ground State Properties and Order Parameters	<b>30</b>
4.2 Finite Temperature Properties	<b>41</b>
4.3 The Magnetic Phase Diagram	<b>57</b>
5 Conclusions	<b>59</b>
References	<b>62</b>

## List of Figures

Figures	page
Figure (3.1): A schematic of the Metropolis algorithm.	24
Figure (3.2): Average internal energy ( $\langle E/g \rangle$ ) per spin as a function of time (MCS/site) for the plane rotator model having long-range dipolar, short-range exchange, and uniform applied magnetic field, in an $N = 104^2$ system.	28
Figure (4.1): Some examples of the dipolar anti-ferromagnetic ground state Spin configurations. In Figure 4.1a the spins are aligned along the x-axis. In Figure 4.1b the spins are ordered at $\pm \frac{\pi}{4}$ to the x-axis. In Figure 4.1c the spins are aligned perpendicular to the x-axis.	31
<b>Figure (4.2):</b> A schematic of the magnetic unit cell showing the four magnetic sub-lattices labeled by $\alpha = 1, 2, 3, 4$ .	32
<b>Figure (4.3):</b> A ground state spin configurations for intermediate values of the applied field $\vec{B}$ , where $\phi_1 = \phi_3$ , and $\phi_2 = \phi_4$ .	34
<b>Figure (4.4):</b> A ground state spin configuration for large values of $\vec{B}$ , where $\phi_1 = \phi_3 = \phi_2 = \phi_4$ .	35
<b>Figure(4.5):</b> The ground state energy per spin as a function of the sub-lattice magnetization angle $\phi$ for different values of $h$ .	39
<b>Figure (4.6):</b> The critical sub-lattice magnetization angle ( $\phi_c$ ) as a function of the applied magnetic field ( $h/g$ ).	40
<b>Figure (4.7):</b> The two thermally averaged order parameters ( $\langle M_{AF} \rangle$ and $\langle M_{FE} \rangle$ ) per spin as a function of both decreasing and increasing the applied magnetic field at $T/g = 0.10$ .	42
<b>Figure (4.8):</b> A plot of $\langle \phi_\alpha \rangle$ , for each of the sub-lattice magnetization, as a Function of both decreasing and increasing the applied magnetic field at $T/g = 0.10$ .	43
<b>Figure (4.9):</b> Snapshots of spin configurations at $T/g = 0.10$ for (a) $h/g = 7.00$ , (b) $h/g = 4.20$ , (c) $h/g = 0.40$ and (d) $h/g = 0.05$ in an $N = 104^2$ system.	44
<b>Figure (4.10):</b> The two thermally averaged order parameters ( $\langle M_{AF} \rangle$ and $\langle M_{FE} \rangle$ ) per spin as a function of increasing and decreasing temperature at $h/g = 1.50$ .	47

Figures	page
<b>Figure (4.11):</b> The specific heat per spin as a function of temperature for heating and cooling the system with $h/g = 1.50$ in $N = 104^2$ system .	48
<b>Figure (4.12):</b> The thermally averaged order parameters ( $\langle M_{AF} \rangle$ ) per spin as a function of increasing and decreasing temperature at $h/g = 1.50$ in $N = 104^2$ and $N = 64^2$ systems .	49
<b>Figure (4.13):</b> The thermally averaged order parameters ( $\langle M_{AF} \rangle$ and $\langle M_{FE} \rangle$ ) as a function of increasing and decreasing temperature $h/g = 8.00$ in an $N = 104^2$ system .	50
<b>Figure (4.14):</b> The heat capacity $C_H$ as a function of increasing and decreasing Temperature for $h/g = 8.00$ in an $N = 104^2$ system .	52
<b>Figure (4.15):</b> The thermally averaged order parameters ( $\langle M_{AF} \rangle$ and $\langle M_{FE} \rangle$ ) as a function of increasing and decreasing temperature for $h/g = 4.75$ in an $N = 104^2$ system .	54
<b>Figure (4.16):</b> The thermally averaged order parameters ( $\langle M_{AF} \rangle$ and $\langle M_{FE} \rangle$ ) as a function of increasing and decreasing temperature for $h/g = 4.75$ in an $N = 104^2$ system around the transition point .	55
<b>Figure (4.17):</b> The heat capacity $C_H$ as a function of increasing and decreasing temperature in $N = 104^2$ system .	56
<b>Figure (4.18):</b> The magnetic phase diagram for the planar system as a function of the applied magnetic field and temperature in an $N = 104^2, 64^2, 32^2$ systems. Region I is the dipolar phase, region II is the ferromagnetic phase and region III is the paramagnetic phase. The simulation points between region I and II indicate the line of first-order transition between the dipolar phase and the ferromagnetic phase; where as the simulation points between region I and region III indicate the line of a second-order transition between the dipolar phase and the paramagnetic phase. The solid line highlights the line where the rounded peaks in the heat capacity data occur due to a remnant of the singularity, which is suppressed by the presence of the applied magnetic field. The filled circle indicates the approximate location of the tri-critical point .	58

**Effects of a Uniform Applied Magnetic Field and Temperature on the  
Magnetic Properties of the Dipolar Anti-ferromagnetic planar System:  
Parametric Study**

**By**

**Naim "Ahmed Rasheed" Mahmoud Malak**

**Supervised by**

**Dr. Abdel-Rahman Mustafa Abu-Labdeh**

**Abstract**

The effects of a uniform external magnetic field, with strength parameter of  $h$ , on the magnetic properties of a two-dimensional square dipolar antiferromagnetic planar system, with sizes  $(104 \times 104, 64 \times 64, 32 \times 32)$ , have been determined for both zero and finite temperatures. In this study, the classical spins are confined to the plane of the system and interact through a nearest neighbor antiferromagnetic exchange interaction, the long-range dipolar interaction, and a uniform external magnetic field along the axis of the lattice. Throughout, the strength of the exchange interaction is assumed to be antiferromagnetic and fixed at  $-1.2g$ , where  $g$  is the strength of the dipolar interaction. At zero temperature, the ground state calculations show that the system switches from ferromagnetic phase (FE phase) to the dipolar antiferromagnetic phase (AF phase) at  $h_0 = 6.00g$  as the applied field is decreased. As the applied field is decreased further, the spin configuration starts to turn antiferromagnetically perpendicular to the applied field in a continuous manner. As the applied field goes to zero, the system favors the dipolar antiferromagnetic in which the spins are aligned perpendicular to the field (AF1 phase). At finite temperature, the magnetic phase diagram for the system has been determined as a function of both  $h$  and  $T$  using Monte Carlo simulations. At low temperatures, the results from simulations show that the system exhibits a first order transition from the

ferromagnetic phase to the dipolar phase (AF phase) as the field is decreased. When the applied field goes to zero, the system favors the dipolar phase in which the spins are ordered at  $\theta = 0$  with the axis of the lattice (AF2 phase). At low fields, the Monte Carlo results indicate that the system exhibits a second order transition from the dipolar antiferromagnetic phase to the paramagnetic phase as the temperature is increased. However, at high fields and for low temperatures the system favors the ferromagnetic phase. As the temperature is increased the system gradually disorders. In addition, Monte Carlo simulation results show that there exists a range of the magnetic field values in which the system exhibits a first order reorientation transition from the dipolar antiferromagnetic phase to the ferromagnetic phase as the temperature is increased.

# **Chapter 1**

## **Introduction**

## Chapter 1

### Introduction

Along the past two decades, there has been an increasing interest in reduced dimensional magnetic systems, stimulated by the wide use of such materials in industrial applications and manufacturing processes. One important class of reduced dimensional magnetic materials is quasi two-dimensional systems. The attractive features of this class of materials for both scientific and technological applications are referred to their magnetic properties, which are different from those of their bulk counterparts. This has recently led to significant technological applications such as magnetic sensors, recording and storage media [1, 2] .

Three important magnetic systems can be considered to be quasi-two-dimensional. The first is ultra thin magnetic films. Ultra thin magnetic films consist of several mono-layers of magnetic atoms deposited on a non-magnetic substrate, such as Ni on Cu(001) substrate [3, 4]. The magnetic spins of such films are observed to be ordered at low temperatures, and show a variety of interesting ordered phases. Among these are the reorientation transitions of magnetization from out-of-plane to in-plane either above critical temperature at constant film thickness [5, 6, 7, 8], or above critical film thickness at constant temperature [5, 6, 9, 10, 11]. A transition from in-plane to out-of-plane has also been observed, as in Ni on Cu(001) substrate and Gd on W(110) substrate [12, 13, 14]. A wide variety of magnetic patterns can also be stabilized in ultra thin magnetic films,

because of the interplay between the perpendicular induced surface anisotropy, the exchange interaction, and the long-range dipolar interaction [15, 16, 17].

Nowadays ferromagnetic thin films are of great interest due to several reasons. First, their wide range of applications in electronics, data storage, processing, recording media, catalysis, biotechnology, and pharmacology [18, 19, 20]. Second, advances in film growth methods [9, 21]. Third, enhancements in characterization methods [5, 7, 8, 22]. In the context of the current work, antiferromagnetic thin films, which are used in spin valve applications [1, 2, 23, 24, 25, 26, 27, 28], is a challenge area of research. Although the technological importance of the spin valve, few research have been done on the antiferromagnetic thin films due to the inability of conventional methods to spatially determine the microscopic magnetic structure of the antiferromagnetic thin films [29]. Recently, this problem has been partially solved by the use of X-ray magnetic linear dichroism spectroscopy [30, 31, 32, 33]. Even though, antiferromagnetic thin films remain an experimental and theoretical challenge.

The second important class of quasi-two-dimensional systems is the layered magnetic compounds as the rare earth (RE) ions in the family compounds  $\text{REBa}_2\text{Cu}_3\text{O}_{7-\delta}$  ( $0 < \delta < 1$ ). These rare earth compounds are suggested to be quasi-two-dimensional systems because their structures consist of the ab-planes of RE ions each of which lie between two double copper oxide layers, and the c-axis is approximately three times as long as

the a and b axes [34, 72]. This class of magnetic materials is very interesting because nearly all rare earth ions in such compounds show antiferromagnetic ordering at low temperatures ( $2\text{K}^\circ$ ), and this ordering phase coexists with the superconducting phase. In the case of  $\text{ErBa}_2\text{Cu}_3\text{O}_7$ , for example, neutron-scattering technique shows that its magnetic spins are ordering within the ab-plane (with Neél temperature  $T_N \approx 0.50\text{K}^\circ$ ). In this case, the magnetic spins are aligned ferromagnetically in the b direction and antiferromagnetically in the a direction. This phase is denoted as the dipolar antiferromagnetic phase (AF1 phase) [36, 37, 38, 39, 40, 41, 42].

The third important class of quasi-two-dimensional systems is the magnetic micro or nano particles; where a large number of publications with different geometries have been considered, including regular arrays of magnetic nano particles such as dots, rings, tubes, and wires [43, 44, 51, 52, 53, 54, 55, 56, 57].

In addition to the basic scientific interest in the magnetic properties of the nanodots, there is evidence that they might be used in the production of new magnetic devices, specially in recording media [60, 61]. Obviously, modern technology demands techniques capable of producing nano meter-sized structure over large areas. A good perspective is the use of nano dots nickel that could store terabyte of data in a computer chip just a few centimeters wide [74]. Recent studies on such structures have been carried out with the aim of determining the stable magnetized state as a function of the geometry of the particles [62, 63]. In particular, the study of highly

ordered arrays of magnetic wires with diameters typically in the range of tens to hundreds of nanometers is a topic of growing interest [64, 65, 66, 67]. The high ordering, together with the magnetic nature of the wires, are fundamental in technological interest, since they can determine the success of patterned media in high-density information storage [69] .

The magnetization of ferromagnetic nano wire arrays has already been studied by magnetic force microscopy (MFM) that, in addition, enables us to gain direct magnetic information of individual nano-objects. In these works, MFM measurements have been carried out by applying magnetic fields on magnetized and demagnetized samples to study the switching behavior of individual nanowires and to obtain the hysteresis loops of the nanowire arrays [64, 50, 70]. In the equilibrium state, it was found that the nanowires exhibit a homogeneous magnetization along the axial direction (with the magnetization of each wire pointing up or down). It appears that the magnetostatic interaction among these wires can play a fundamental role in the magnetization reversal processes and domain structures of each wire, which consequently affect the magnetic properties of the system. In particular, it was pointed out that the dipolar interaction between such wires has a similar effect on its magnetic properties as do classical spins interacting through long range dipolar interaction [58]. So the interaction among these wires can be best described by a two-dimensional model. Moreover, a reorientation transition has been predicted and observed in micro or nano magnetic dot systems [59].

The development of materials with certain characteristics to a specific application requires a sufficient understanding of their microscopic interactions that are affected by some factors such as the composition and preparation of the system. For example, the tasks of using ultra thin magnetic films in data storage aspects requires that the magnetization of the film be set and read with a high degree of accuracy. Further more, variations in the composition of the film can be used to manipulate some properties such as sensitivity to an external field [89]. Consequently, the stability of magnetic ordering in reduced dimensional systems is affected by various factors due to the type and nature of interactions that are presented in a particular system. Most of the recent explosive growth in electromagnetic media, therefore has been referred to the new discoveries and better understanding of the magnetic and electronic properties of low-dimensional systems .

In addition to the dimensionality of the lattice, the spin dimensionality is an important factor in determining the magnetic properties of low-dimensional magnetic systems. Theoretical studies have divided such magnetic systems into Ising model (in which the spins are constrained to be oriented perpendicular to the plane of the system due to the strong perpendicular magnetic surface anisotropy), plane rotator model (in which the spins are confined to the plane of the system due to the strong planar surface anisotropy), and the anisotropic Heisenberg model (in which the spins have three dimensional components due to a finite value of magnetic surface anisotropy). A realistic theoretical model of low-

dimensional magnetic systems must include the exchange interaction, the dipolar interaction, and the magnetic surface anisotropy [71]. Despite its small amount, the long-range dipolar interaction plays essential role in two dimensional magnetic systems due to its long range character and its anisotropic nature. In the two dimensional plane rotator system, for example, it was found that the short-range exchange interaction is insufficient for establishing a spontaneous magnetization at any finite temperature [76, 77]. Different and interesting behavior appears in the plane rotator model when the dipolar interaction is included. Using the Luttinger and Tisza method, Belobrove et al reported that the ground state (i.e., zero temperature state) of the pure dipolar planar system on a square lattice is continuously degenerate and consists of four sublattices, where the spins of these sublattices make angles  $\phi$ ,  $2\pi-\phi$ ,  $\pi-\phi$ ,  $\pi+\phi$  and with the positive x-axis counterclockwise ( $\phi$  being arbitrarily) [78, 79].

Using both the mean field mean-field theory and Monte Carlo simulations, Zimmerman et al have confirmed the existence of such continuous degeneracy in a pure dipolar planar model on the honeycomb lattice [80]. Later on, Henly (who introduced the concept of “order from disorder”) concluded that fluctuations such as thermal fluctuations and dilution, or applied magnetic field break the degeneracy of the ground state [81, 82]. Moreover, Parakash and Henley studied the two-dimensional plane rotator system on both square and honeycomb lattices with nearest neighbor dipolar interaction [83]. They found that thermal fluctuations, dilution and uniform applied magnetic field break the continuous

degeneracy of the ground state to a discrete fourfold symmetry in the case of a square lattice and to a discrete six-fold symmetry in the case of the honeycomb lattice. They also found that, in the case of the square lattice, the thermal fluctuations favor a dipolar antiferromagnetic phase in which spins are aligned ferromagnetically along one of the two axes of the lattice and antiferromagnetically along the other axis (AF1 phase), while the dilution favors a dipolar antiferromagnetic phase in which the spins are ordered at  $45^\circ$  to the x-axis (AF2 phase). For the case of a uniform applied magnetic field along the x-axis, they found that this field favors a dipolar antiferromagnetic phase in which the spins are ordered ferromagnetically along the x-axis and antiferromagnetically along the other axis (AF1 phase, which is perpendicular to the applied field).

The two-dimensional square planar system with pure long-range dipolar interaction was studied at finite temperature by Monte Carlo simulations as well as linearized spin-wave approximations [84, 85]. Both studies also showed a long-range magnetic order in such systems. The two dimensional square planar system having the long-range dipolar and the short-range antiferromagnetic interactions was investigated by both Monte Carlo simulations and linearized spin-wave approximations [86, 87]. These two studies concluded that thermal fluctuations break the degeneracy of the ground state and lead to a long range magnetic order. In addition, the two studies showed that the characteristics of the ordered phase depend on the strength of the exchange parameter. At low temperatures, the results show that a first order transition from the dipolar antiferromagnetic phase to the

simple antiferromagnetic phase (AA phase) can occur as the antiferromagnetic parameter is increased. The results also show that the dipolar phase consists of two distinct phases AF1 and AF2. While AF1 phase occurs in the two regions where  $\mu < \mu_c$  and  $\mu > \mu_c$ , AF2 occurs in the region  $\mu < \mu_c$ .

Recently, Abu-Labdeh et al investigated the two-dimensional planar system on a square lattice having the long-range dipolar interaction and a uniform applied magnetic field along the x-axis for both zero and finite temperature [88]. From Monte Carlo simulations, the magnetic phase diagram was determined for this system as a function of the applied field and temperature. At low temperatures and for low values of the applied field, Monte Carlo results show AF1 phase in which the spins are aligned perpendicular to the field. As the external field is increased the dipolar order parameter decreases continuously until the system undergoes a transition to the ferromagnetic phase (FE phase).

While extensive work has been done on the behavior of reduced-dimensional ferromagnetic systems, few systematic works has been done on reduced-dimensional antiferromagnetic systems. In particular, little is known about the effects that arise from the interplay of the dipolar, exchange, magnetic surface anisotropy, and uniform external magnetic field in the low-dimensional antiferromagnetic systems. To get a better understanding of both the micro and macroscopic properties of the magnetic phenomena within the low-dimensional antiferromagnetic systems, this study focuses on the effects of a uniform external magnetic

field and temperature on the magnetic behavior of the classical two-dimensional dipolar antiferromagnetic plane rotator system. For zero temperature analytic method is used, while at finite temperatures a number of Monte Carlo simulations are carried out. Throughout, the exchange interaction parameter  $J$  is assumed to be antiferromagnetic with a fixed value ( $J = -1.2 g$ , where  $g$  is the strength of the dipolar parameter). In addition, the applied magnetic field is assumed to be uniform and parallel to the x-axis of the square lattice .

The outline of this thesis is as follows. In Chapter two we will present the planar model in general terms including the dipole-dipole interaction, exchange interaction, and uniform external magnetic field. In Chapter three, the basic methods behind Monte Carlo simulation technique and the computational aspects will be introduced. In Chapter four, the results of the system of interest for both zero and finite temperatures are presented and discussed. Finally, the conclusion is given in chapter five.

## **Chapter 2**

### **The Model in General Terms**

## Chapter 2

### The Model in General Terms

In this study, the model of interest is a square planar model, in which the two in- plane directions of the square lattice are denoted by  $\hat{x}$  and  $\hat{y}$ . Each lattice site is associated with an ion which has a total magnetic moment  $\vec{\mu}$ , and a total spin  $\vec{S}$ . The system, therefore, is composed of  $N$  ions arranged on a square lattice of length  $L$ , such that  $N = L \times L$ . The magnetic moments and spins are confined to rotate freely in the plane of the system. The ions of the present system are assumed to interact through the long-range dipolar interaction ( $E_{dd}$ ), nearest neighbor antiferromagnetic exchange interaction ( $E_{ex}$ ), and uniform external magnetic field ( $E_h$ ) which represents the contribution of a uniform external magnetic field along the  $x$ -axis of the lattice. So that the total energy  $E$  of the system can be written as

$$E = E_{dd} + E_{ex} + E_h \quad (2.1)$$

The first term of Equation 2.1 corresponds to the dipole-dipole interaction that are always present between magnetic moments. As stated before, the dipolar interaction has a long-range character, and it is anisotropic. The contribution of the dipolar interaction is

$$E_{dd} = \frac{1}{2} \sum_{i \neq j} \left( \frac{\vec{\mu}_i \cdot \vec{\mu}_j}{r_{ij}^3} - 3 \frac{(\vec{\mu}_i \cdot \vec{r}_{ij})(\vec{\mu}_j \cdot \vec{r}_{ij})}{r_{ij}^5} \right) \quad (2.2)$$

where  $\vec{\mu}_i$  is the classical magnetic moment at the lattice site  $i$ ,  $\vec{r}_{ij}$  is the vector connecting site  $i$  to site  $j$ , and the sum is over all possible pairs of sites in the lattice except  $i = j$ .

The second term of Equation 2.1 is the nearest neighbor exchange interaction. Ferromagnetism and antiferromagnetism are based on variations of the exchange interaction, which is a consequence of the Pauli principle and the Coulomb interactions. The simplest case of the exchange interaction is due to two ions with spins  $\vec{S}_1$  and  $\vec{S}_2$ , which is given by

$$E_{ex} = -\mathfrak{J} \vec{S}_1 \cdot \vec{S}_2 \quad (2.3)$$

where  $\mathfrak{J}$  is the exchange constant which depends on the distance between the spins, and it is determined by the overlap integrals. For positive parameter  $\mathfrak{J}$ , a parallel spin orientations is favored, which leads to ferromagnetic state; while for negative exchange parameter, an antiparallel spin orientations is preferred, which leads to a simple antiferromagnetic state. In contrast to the dipolar interaction, the exchange interaction has features of short-range characters, and it has an isotropic nature. For a system of  $N$  spins, the exchange energy is then given by

$$E_{ex} = -\mathfrak{J} \sum_{\langle i, j \rangle} \vec{S}_i \cdot \vec{S}_j \quad (2.4)$$

where the sum is over all nearest neighbor pairs, and  $\vec{S}_i$  is the classical spin vector at site  $i$ . The last term of Equation 2.1 refers to the Zeeman energy, which arises from the interaction of an applied magnetic

field with the magnetic moments. As mentioned earlier, it has an important role in characterizing the development of materials in specific features. For example, the fabrication of magnetic thin films, that are very sensitive to the application of an external magnetic field needs a detailed understanding of their microscopic interactions. In addition, the wide use of technological applications such as data storage often requires manipulation of the magnetic structure by an external magnetic field [89]. The contribution of this term to the total energy of the system is

$$E = -B \sum_i \mu_i^x \quad (2.5)$$

where  $B$  is the strength of a uniform external magnetic field in the direction of the  $x$ -axis, and  $\mu_i^x$  is the component of a magnetic moment in the direction of the applied magnetic field. With Equations 2.2, 2.4, and 2.5, Equation 2.1 reads

$$E = \frac{1}{2} \sum_{i \neq j} \left( \frac{\vec{\mu}_i \cdot \vec{\mu}_j}{r_{ij}^3} - 3 \frac{(\vec{\mu}_i \cdot \vec{r}_{ij})(\vec{\mu}_j \cdot \vec{r}_{ij})}{r_{ij}^5} \right) - \mathfrak{S} \sum_{\langle i, j \rangle} \vec{S}_i \cdot \vec{S}_j - B \sum_i \mu_i^x \quad (2.6)$$

In order to carry out Monte Carlo simulations, Equation 2.6 should be expressed in terms of dimensionless quantities. Therefore, we define a set of two-dimensional classical unit vectors  $\{\vec{\sigma}\}$  such that

$$\vec{\mu}(r_i) \equiv \mu_{eff} \vec{\sigma}(r_i) \quad (2.7)$$

and

$$\vec{S}(\vec{r}_i) \equiv S_{eff} \vec{\sigma}(\vec{r}_i) \quad (2.8)$$

Where

$$\left| \vec{\sigma}(\vec{r}_i) \right| = 1 \quad (2.9)$$

In addition, all distances are scaled by the lattice constant  $a$ , such that

$$\vec{R}_i \rightarrow \frac{\vec{r}_i}{a}$$

With these definitions, Equation 2.6 is then reduced to

$$\begin{aligned} E = & \frac{\mu_{eff}^2}{2a^3} \sum_{i \neq j} \left( \frac{\vec{\sigma}_i \cdot \vec{\sigma}_j}{R_{ij}^3} - 3 \frac{(\vec{\sigma}_i \cdot \vec{R}_{ij})(\vec{\sigma}_j \cdot \vec{R}_{ij})}{R_{ij}^5} \right) \\ & - \mathfrak{S} S_{eff}^2 \sum_{\langle i, j \rangle} \vec{\sigma}_i \cdot \vec{\sigma}_j - B \mu_{eff} \sum_i \sigma_i^x \end{aligned} \quad (2.10)$$

For simplicity, we define new coupling parameters

$$g = \frac{(\mu_{eff}^2)}{2a^3} \quad (2.11)$$

$$J = \mathfrak{S} S_{eff}^2 \quad (2.12)$$

$$h = B \mu_{eff} \quad (2.13)$$

where  $g$ ,  $J$ , and  $h$ , respectively, represent the strength parameters of the dipolar, exchange and applied field interactions. Substituting Equations 2.11, 2.12, and 2.13 into Equation 2.10 yields

$$\begin{aligned}
E = & g \sum_{i \neq j} \left( \frac{\vec{\sigma}_i \cdot \vec{\sigma}_j}{R_{ij}^3} - 3 \frac{(\vec{\sigma}_i \cdot \vec{R}_{ij})(\vec{\sigma}_j \cdot \vec{R}_{ij})}{R_{ij}^5} \right) \\
& - J \sum_{\langle i, j \rangle} \vec{\sigma}_i \cdot \vec{\sigma}_j - h \sum_i \sigma_i^x
\end{aligned} \tag{2.14}$$

In the present study, the parameters  $J$  and  $h$  are measured in units such that  $g = 1$ , and the exchange interaction is assumed to be antiferromagnetic with a fixed value (i.e.,  $J = -1.2g$ ).

Since the dipolar energy is slowly convergent, it is efficient to apply the Ewald summation technique for calculating its sum. The main idea behind this technique is to separate the dipolar energy into two parts.

The first part is localized and rapidly convergent in real space, while the second part is a long-range component and rapidly convergent in momentum space. However, the details of this technique is described in earlier work [90, 91].

**Chapter 3**  
**Monte Carlo Simulations and**  
**the Computational Details**

## Chapter 3

### Monte Carlo Simulations and the Computational Details

While the task of statistical mechanics at equilibrium is to calculate thermal averages, the problem of the many particle system is best treated by means of computational methods. Nowadays, computer simulations have become a rich source of scientific research that support both theory and experiment in a variety of fields and subjects. The advantage of simulations is that one can get a better understanding by switching off one or more physical parameters that are simultaneously affect the real systems. One remarkable simulation method is the Monte Carlo technique. From a historical point of view, the first large scale Monte Carlo work carried out dates back to the middle of the twentieth century. The earliest published work on Monte Carlo is perhaps the paper of Metropolis and Ulam [93] in the year 1949. Monte Carlo (MC) technique is based on random numbers. For carrying out a MC simulation, we require a sequence of numbers, which are random, independent, real and uniformly distributed in the range 0 to 1. The aim of MC simulations, therefore, is to evaluate thermal averages by statistically sampling the significant region of their phase space using a computer.

In this Chapter, we will introduce (in brief) the fundamentals of Monte Carlo simulations, including importance sampling, transition probability, detailed balance, and the Metropolis algorithm. For more details readers may return to many references

and texts as in [92, 93, 94, 95, 96, 97].

### 3.1 Importance Sampling, Detailed Balance, and Metropolis Algorithm

In thermodynamics, there are two main categories of measurements that are performed in computational statistical physics. They are called mechanical quantities, and entropic (or thermal quantities). Examples of mechanical quantities are internal energy ( $U$ ) and pressure ( $P$ ), while examples of entropic quantities are the free energy ( $F$ ) and entropy ( $S$ ). These two categories of thermodynamic quantities are distinguished by their relations to the partition function  $Z$ . For example  $U$  is given

by

$$U = K_B T^2 \frac{\partial}{\partial T} \ln(Z), \quad (3.1)$$

while  $F$  is given by

$$F = -K_B T \ln(Z), \quad (3.2)$$

where  $T$  is the temperature, and  $k_B$  is the Boltzmann constant.

In the canonical ensemble, the observable thermal quantity  $Q$  of a system can be calculated as

$$\langle Q \rangle = \frac{\sum_{\lambda} Q_{\nu\lambda} \exp\left[-\frac{E_{\nu\lambda}}{K_B T}\right]}{\sum_{\lambda} \exp\left[-\frac{E_{\nu\lambda}}{K_B T}\right]}, \quad (3.3)$$

where  $E_{\nu_\lambda}$  is the energy of the system in state  $\nu_\lambda$ ,  $Q_{\nu_\lambda}$  is the value of  $Q$  at some state  $\nu_\lambda$ , and

$$P(\nu_\lambda) \propto \exp[-E_{\nu_\lambda}/K_B T] \quad (3.4)$$

is the Boltzmann probability. In general, the exact evaluation of Equation 3.3 is impossible. For example, the Ising spin system of 100 spins have  $2^{100} \approx 10^{30}$  states. If we assume, optimistically, that it takes a nano second to generate a spin configuration, the total time required to sample all the spin configurations is nearly of the order of thirty thousand billion years. Therefore, an approximation method is needed to estimate  $\langle Q \rangle$ . One approximation method is to evaluate the quantity  $\langle Q \rangle$  by summing Equation 3.3 over a large, but finite number of states. These states are selected according to the Boltzmann probability distribution  $P(\nu)$ , in which they are statistically significant. This method is called the importance sampling.

The significant states are selected using a Markov process. In this process, state  $\nu_{\lambda+1}$  is generated from previous state  $\nu_\lambda$  through a transition probability  $W(\nu_\lambda \rightarrow \nu_{\lambda+1})$ , such that the distribution function of the states generated by the Markov process is given by the Boltzmann distribution. Markov process, therefore, should satisfy the following four conditions.

- The state  $\nu_{\lambda+1}$  is generated every time it is determined by the state  $\nu_\lambda$ .
- The transition probability should satisfy the condition

$$\sum_{\lambda} W(\nu_\lambda \rightarrow \nu_{\lambda+1}) = 1. \quad (3.5)$$

This condition is so called the condition of normalization.

- Reaching any state of the system from any other state is possible if the program is run for a long enough time. This condition is so called the condition of ergodicity.
- At equilibrium, the rate at which the system makes transition into or out of any state  $\nu$  must be equal. This condition is so called condition of the detailed balance, and is given by

$$P(\nu_\lambda)W(\nu_\lambda \rightarrow \nu_{\lambda+1}) = P(\nu_{\lambda+1})W(\nu_{\lambda+1} \rightarrow \nu_\lambda), \quad (3.6)$$

or

$$\frac{W(\nu_\lambda \rightarrow \nu_{\lambda+1})}{W(\nu_{\lambda+1} \rightarrow \nu_\lambda)} = \frac{P(\nu_{\lambda+1})}{P(\nu_\lambda)} = \exp[-(E_{\lambda+1} - E_\lambda)]. \quad (3.7)$$

Equation 3.7 implies that the transition probability ratio for moving from state  $\nu_\lambda$  to state  $\nu_{\lambda+1}$  depends only on the energy change

$$\Delta E = E_{\lambda+1} - E_\lambda \quad (3.8)$$

One efficient method for the transition probability that satisfies Equation 3.7 is the Metropolis algorithm [97]. In this algorithm the transition probability from state  $\nu_\lambda$  to state  $\nu_{\lambda+1}$  reads

$$W(\nu_\lambda \rightarrow \nu_{\lambda+1}) = \begin{cases} \exp[-\Delta E], & \text{if } E_{\nu_{\lambda+1}} \leq E_{\nu_\lambda} \\ \exp[-\Delta E] \frac{P(\nu_{\lambda+1})}{P(\nu_\lambda)}, & \text{if } E_{\nu_{\lambda+1}} > E_{\nu_\lambda} \end{cases} \quad (3.9)$$

Equation 3.9 indicates that the transition to the new state  $\nu_{\lambda+1}$  is accepted if its energy is lower than or equal to the present state  $\nu_{\lambda}$ . However, if the state  $\nu_{\lambda+1}$  has a higher energy than the state  $\nu_{\lambda}$  then there is, still, a possibility to accept it. To accept a new state which has a higher energy than the present state, we choose a random number  $Z$  between 0 and 1. If the transition probability is greater than  $Z$ , then we accept the new state  $\nu_{\lambda+1}$ , otherwise the new state is rejected and the system stays in the present state  $\nu_{\lambda}$ . In moving from  $\nu_{\lambda}$  to  $\nu_{\lambda+1}$ , there are many choices. One common and efficient choice is to change only one degree of freedom of the system (such as rotating a single spin at an angle  $\phi$  to a new angle  $\phi'$  in the case of the plane rotator system).

The optimal Metropolis algorithm used in the present study proceeds according to the following ten steps:

1. Choose an initial state,  $\nu_{\lambda} = \{\vec{\sigma}_0\}$ , of the system,
2. Randomly select the target spin,  $\vec{\sigma}_i$ , where  $i \in (1, 2, 3, \dots, N = L \times L)$ ,
3. Generate a new state,  $\nu_{\lambda+1}$ , randomly by changing the orientation of the

selected  $\vec{\sigma}_i$  to  $\vec{\sigma}'_i$  such that

$$\vec{\sigma}'_i = \vec{\sigma}_i + \mu \Delta \vec{\sigma}_i \quad (3.10)$$

4. Compute the energy difference,  $\Delta E$ , between the new state and the old state,
5. Calculate the Transition probability according to Equation 3.9,
6. Generate a uniform distribution number  $Z$  between 0 and 1,
7. Compare  $Z$  with the Calculated  $W(\nu_{\lambda} \rightarrow \nu_{\lambda+1})$ . If  $W(\nu_{\lambda} \rightarrow \nu_{\lambda+1})$  is greater

than  $Z$  accept the move, otherwise leave the spin as it is and retain the old spin configuration,

8. Repeat steps 2-7 as necessary,
9. Store the required observable quantities of the system every  $n^{\text{th}}$  Monte Carlo steps per lattice site ( $MCS/site$ ) to calculate the averages,
10. Calculate the required observable quantities of the system using the

Simple arithmetic average

$$\langle Q \rangle_M = \sum_{\lambda=1}^M \frac{Q_{\nu\lambda}}{M} \quad (3.11)$$

where  $Q_{\nu\lambda}$  is the value of the observable quantity  $Q$  at the state  $\nu\lambda$  and  $M$  is the total number of the Monte Carlo steps per lattice site. Equation 3.11 indicates that  $\langle Q \rangle_M$  becomes a more and more accurate estimate as the number of the Monte Carlo steps per site (i.e.,  $M$ ) is increased.

The Metropolis algorithm is shown schematically in Figure 3.1.

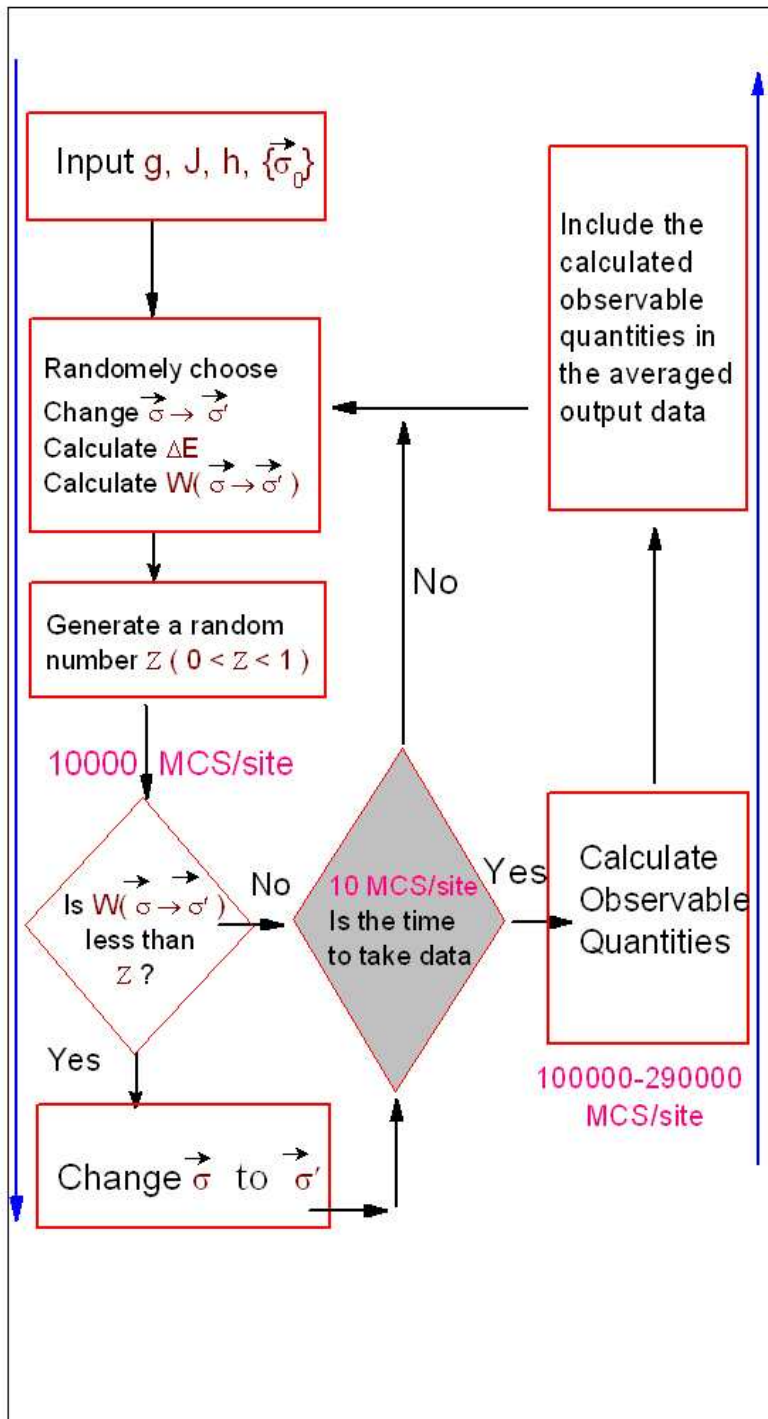


**Figure (3.1):** A schematic of the Metropolis algorithm.

### 3.2 Computational Aspects

Throughout this research, the finite temperature MC Simulations for the plane rotator model are carried out via super-computing machine clusters through Western Canada Research Grid *WestGrid* and Shared Hierarchical Academic Research Computing Network *SHARCNET*.

The finite system is simulated for different lattice sizes;  $N = 32^2, 64^2, 104^2$ , and is treated as an infinite plane of replicas by imposing suitable periodic boundary conditions [72, 98, 88, 99]. As an illustration, the first site in a row in the square lattice is considered as the right nearest neighbor of the last site in the same row and the last site in a row is considered as the left nearest neighbor of the first site in the same row. The same holds for the top and bottom sites in each column. In addition, the Ewald summation technique is used to sum over the replicas [72]. Indeed, the simulations are based on the standard Metropolis algorithm. However, the code used in this study was originally written by MacIsaac and his co-workers [100, 102], and modified by Abu-Labdeh and his co-workers [102].

Data are collected from Monte Carlo simulations through two stages. In one, temperature is fixed at a certain value and the external field is varied gradually in steps of 0.05. In the other, the external field is fixed at a certain value and the temperature is varied in steps of 0.05. Phase transitions occur when the properties of the system is changed. From the transition points, the magnetic phase diagram of the system has been determined as a function of both temperature and applied magnetic field.

Detailed coverage of the phase behavior are performed with  $L = 32$ , and the results are confirmed with  $L = 64$  and  $104$ . For each Monte Carlo simulation, the number of Monte Carlo steps per unit site (MCS/site) that is required to bring the system into equilibrium is estimated, from the plot of the internal energy versus time (Figure 3.2), to be  $10^4$  MCS/site. The number of samples used to calculate the averages, however, ranged from  $14 \times 10^4$  MCS/site at high values of temperature for the  $104 \times 104$  system to  $29 \times 10^4$  MCS/site at low temperature for the  $32 \times 32$  system.

For a wide range of temperatures selected arbitrarily, in each Monte Carlo simulation job, the external magnetic field  $h$  is applied parallel to the  $x$ -axis of the lattice and decreased gradually in steps of  $0.05$  throughout the simulation process. It is worth noting that the simulation is initially performed at  $h = 10 g$ , in which the spins are aligned parallel to the applied field. This is more effective to be introduced as an initial state of spins rather than picking them up at random in order to start the Monte Carlo simulation jobs. When the job is completed by reaching  $0$  field, the Monte Carlo simulation job is then reversed in steps of  $0.05$ . (i.e., the applied field is increased in steps of  $0.05$ ). The final state of that simulation at  $h/g$  would then be used as the initial state for the simulation at  $h/g \pm 0.05$ .

By the same manner described in decreasing and increasing the applied field, the system is simulated again for cooling and heating over a wide range of applied field values selected arbitrarily. This time, the simulation is initially performed at  $T/g = 8.00$  in which the spins are in the disordered

phase, and then the temperature is decreased in steps of 0.05. When the run is completed by reaching very low value of temperature ( $T = 0.05$  g), the Monte Carlo simulation run is then reversed (i.e., the temperature is increased in steps of 0.05). Again, the final state of that simulation at  $T/g$  would then be used as the initial state for the simulation at  $T/g \pm 0.05$ .

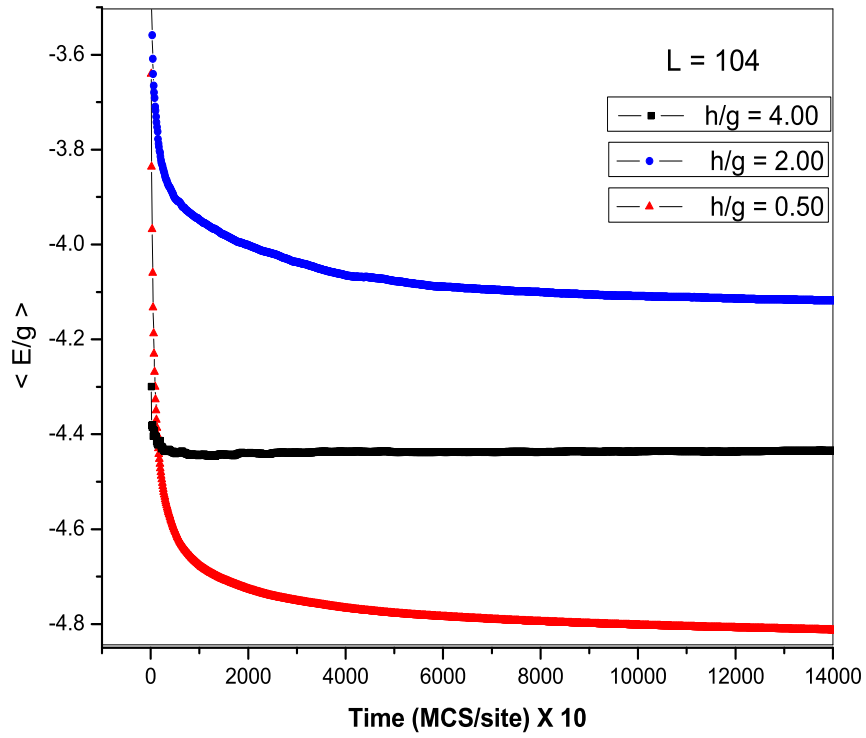


**Figure (3.2):** Average internal energy ( $\langle E/g \rangle$ ) per spin as a function of time (MCS/site) for the plane rotator model having long-range dipolar, short-range exchange, and uniform applied magnetic field, in an  $N = 104^2$  system.

**Chapter 4**  
**Results and Discussion**

## Chapter 4

### Results and Discussion

In this chapter, we present and discuss the magnetic properties of a planar system on a square lattice with lattice sizes  $32 \times 32$ ,  $64 \times 64$ , and  $104 \times 104$ . As mentioned before, in the present system the long-range, short-range, and uniform applied magnetic field are considered. In addition, the strength of the exchange parameters is fixed at  $J = -1.2g$ .

In the following section, the ground state properties and the order parameters of the dipolar anti ferromagnetic and ferromagnetic phases are presented and discussed. The finite temperature properties of the system follow in section 4.2. The chapter closes by the simulations including the magnetic phase diagram.

#### 4.1 Ground State Properties and Order Parameters

In the case of the pure dipolar system ( $h = 0, J = 0$ ), it has been found by several authors that the ground state spin configuration has the spins aligned in the plane of the system and it is continuously degenerate [103, 104, 105]. This ground state is called the dipolar antiferromagnetic state, and denoted by the  $AF$  phase. Some examples of the dipolar antiferromagnetic ground state spin configurations are shown in Figure 4.1. Other ground state spin configurations can be generated by a transformation which continuously maps the spin configurations shown in Figure 4.1a into the spin configuration Figure 4.1c by changing the angle  $\phi$  shown in Figure 4.2 [105]. The fact that the dipolar antiferromagnetic

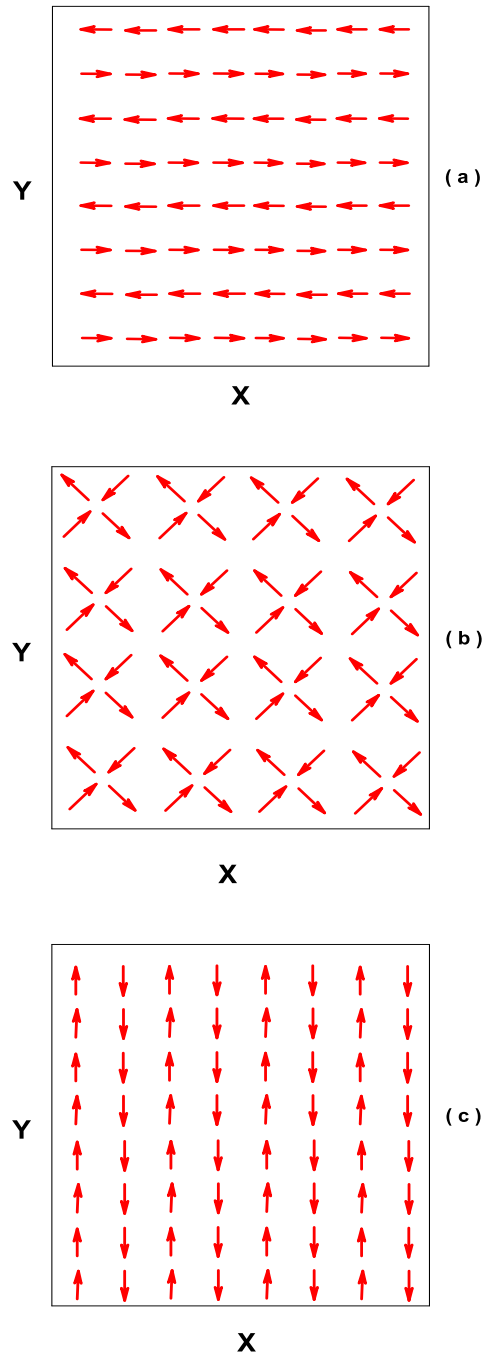


**Figure (4.1):** Some examples of the dipolar anti-ferromagnetic ground state Spin configurations. In Figure 4.1a the spins are aligned along the  $x$ -axis. In Figure 4.1b the spins are ordered at  $\pm \frac{\pi}{4}$  to the  $x$ -axis. In Figure 4.1c the spins are aligned perpendicular to the  $x$ -axis.

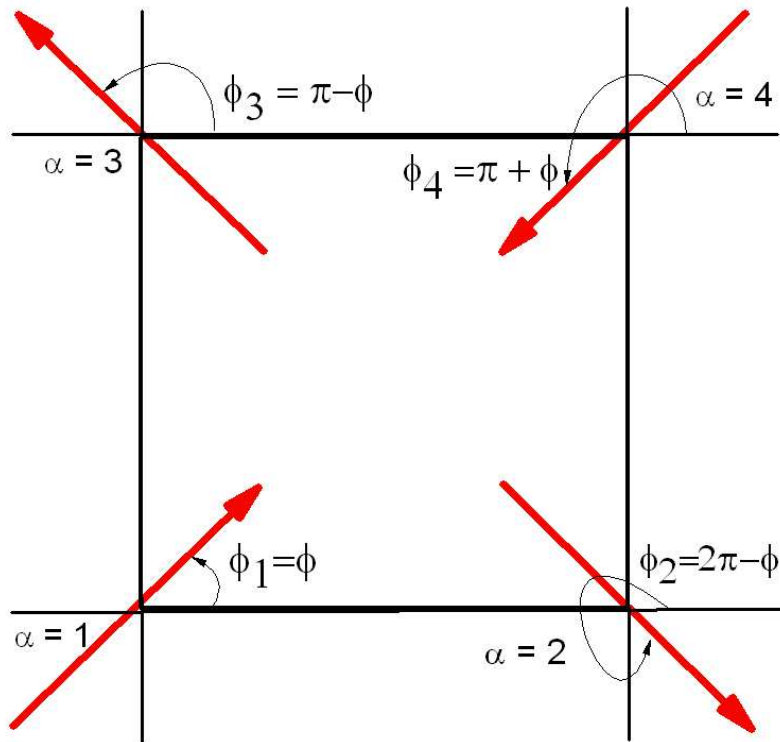


**Figure (4.2):** A schematic of the magnetic unit cell showing the four magnetic sub-lattices labeled by  $\alpha = 1, 2, 3, 4$ .

phase is continuously degenerate is surprising because the dipolar interaction is variant under rotation.

It was pointed out that the addition of a small antiferromagnetic exchange interaction ( $|J| < 3.2 g$ ) does not break the degeneracy of the ground state spin configurations of the pure dipolar system [72, 106]. In contrast, it was found that the addition of a small uniform external magnetic field along the  $x$ -axis breaks the degeneracy of the ground state spin configurations, and leads to a dipolar configuration in which the spins are fully ordered antiferromagnetically perpendicular to the direction of the field as shown in Figure 4.1c [107, 88]. As the applied field is increased, Abu-Labdeh *et al.* [88] found that the spin configuration starts to turn ferromagnetically parallel to the applied field in a continuous manner as shown in Figure 4.3. If the strength of the applied field is sufficiently large ( $h > 1.164 g$ ), they found that the ground state spin configuration switches to a ferromagnetic phase, in which the spins are aligned parallel to the applied field as shown in Figure 4.4. This state is denoted by the *FE* phase. Therefore, the competition between the dipolar and the applied field can lead to a reorientation transition at zero temperature.

Since this study focuses on a square planar system, which includes the long-range dipolar interaction, the short-range exchange interaction, and the applied field, order parameters for the dipolar antiferromagnetic and ferromagnetic states are needed here. In order to establish the order

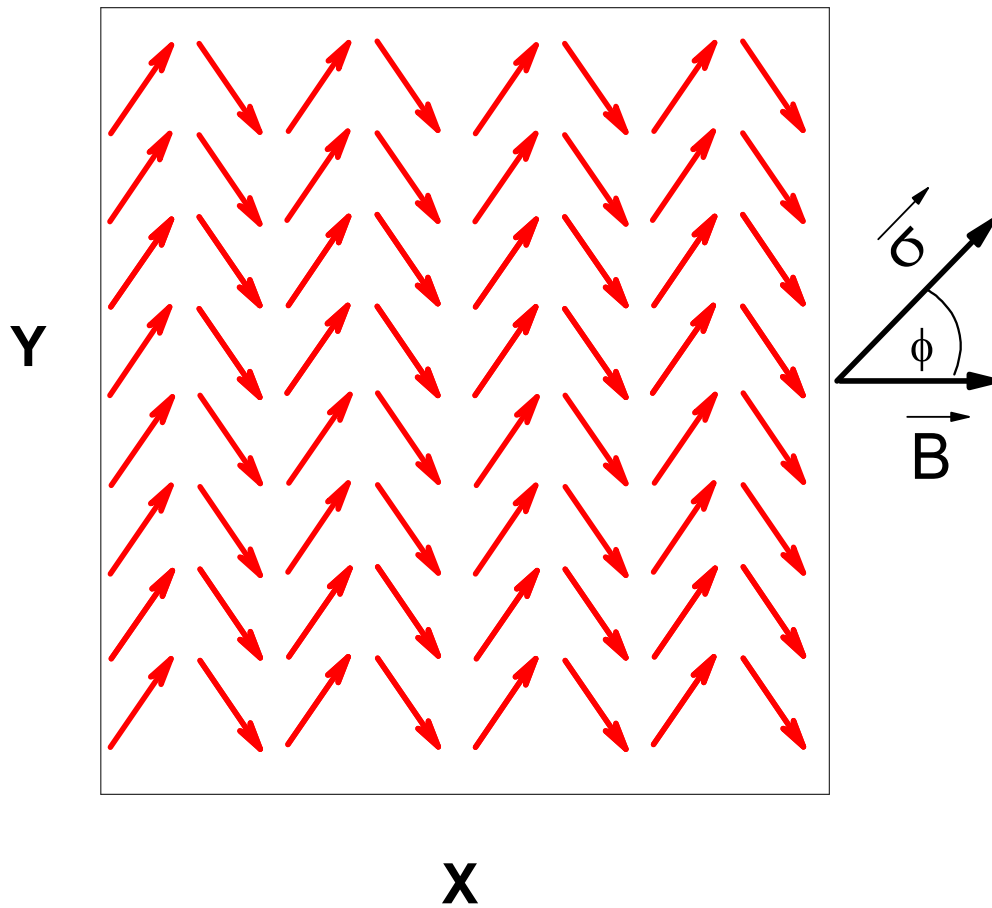


**Figure (4.3):** A ground state spin configurations for intermediate values of the applied field  $\vec{B}$ , where  $\phi_1 = \phi_3$ , and  $\phi_2 = \phi_4$ .

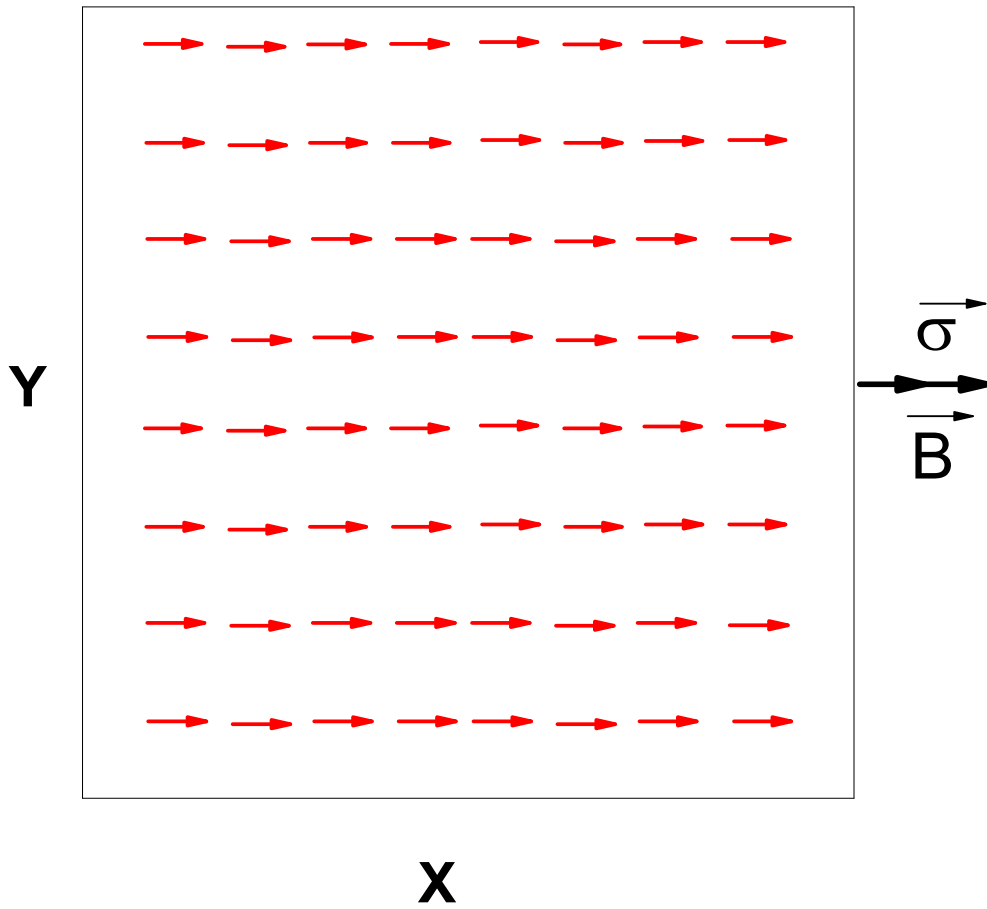


**Figure (4.4):** A ground state spin configuration for large values of  $\vec{B}$ , where  $\phi_1 = \phi_2 = \phi_3 = \phi_4 = 0^\circ$ .

parameters for the present system, the square lattice is subdivided into four sublattices, labeled by an index  $\alpha = 1, 2, 3, 4$  as shown in Figure 4.2. For each sublattice a corresponding sublattice magnetization  $\sim M^\alpha$  is

defined as

$$\vec{M}_\alpha = \frac{4}{N} \left[ \sum_{\vec{r}_\alpha} \sigma^x(\vec{r}_\alpha) \right] \hat{x} + \frac{4}{N} \left[ \sum_{\vec{r}_\alpha} \sigma^y(\vec{r}_\alpha) \right] \hat{y} \quad (4.1)$$

Two order parameters ( $M_{AF}$  and  $M_{FE}$ ) are constructed from Equation 4.1 as

$$M_{AF} = \left| \frac{1}{4} [(M_1^x + M_2^x - M_3^x - M_4^x) \hat{x} + (M_1^y + M_3^y - M_2^y - M_4^y) \hat{y}] \right| \quad (4.2)$$

and

$$M_{FE} = \left| \frac{1}{4} [(M_1^x + M_2^x + M_3^x + M_4^x) \hat{x} + (M_1^y + M_3^y + M_2^y + M_4^y) \hat{y}] \right| \quad (4.3)$$

The order parameter  $M_{AF}$  characterizes ordering in the ground state corresponding to the pure dipolar antiferromagnetic phase, while the order parameter  $M_{FE}$  characterizes ordering in the ground state corresponding to the pure ferromagnetic phase. For the pure dipolar antiferromagnetic phase,

$$M_{AF} = 1 \quad (4.4)$$

$$M_{FE} = 0, \quad (4.5)$$

while for the ferromagnetic phase,

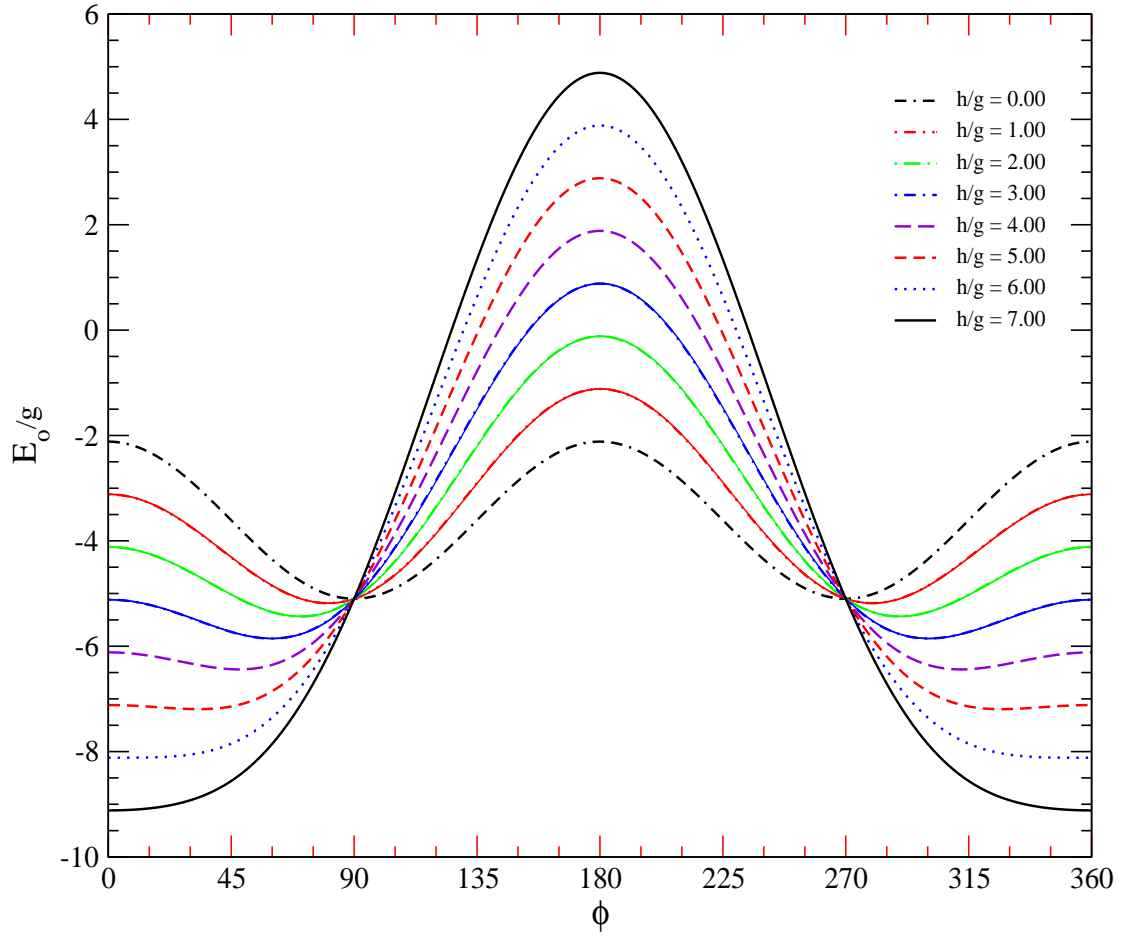
$$M_{AF} = 0 \quad (4.6)$$

$$M_{FE} = 1 \quad (4.7)$$

By restricting the system to the action of the classical Hamiltonian given by Equation 2.14, the ground state energy of the system is calculated as a function of the sublattice magnetization angle  $\phi$  at different values of  $h$ . When  $\phi = 0^\circ$ , the spins are aligned along the positive  $x$ -axis, and as  $\phi$  is varied spins in even numbered columns are rotated clockwise as shown in Figure 4.3, while those in odd numbered columns are rotated counterclockwise. So that for  $\phi = 90^\circ$  spins in odd numbered columns are aligned along the  $\pm y$  axis, while spins in even numbered columns are aligned along the  $-y$  axis as shown in Figure 4.1c.

The results for the ground state energy,  $E_0(\phi)$  are shown in Figure 4.5 for different values of  $h$ . Figure 4.5 indicates that for a fixed value of  $h$  the ground state energy is a minimum at a certain sublattice magnetization angle,  $\phi_c$ . By assigning the local minima for the curves shown in Figure 4.5 and from other similar curves,  $\phi_c$  is plotted as a function of  $h$  as shown in Figure 4.6. From Figure 4.6, we conclude that at zero temperature and for large values of the external field the ferromagnetic state along the applied field is energetically favored. However, at  $\frac{h_0}{g} = 6.00 \pm 0.20$  the spin configuration starts to turn antiferromagnetically perpendicular to the applied field in a continuous manner as shown in Figure 4.3. At very small magnetic field, the spins are fully ordered antiferromagnetically perpendicular to the field as shown in Figure 4.1c.

This result is similar with what Prakash and Henley pointed out for a truncated dipole-like interaction [107], and with what Abu-Labdeh *et al* pointed out for a long-range dipolar interaction [88]. Although the addition of a small exchange interaction does not change the behavior of the spins at zero temperature, it shifts the location of the transition between the ordered phases to a higher value of the applied field.



**Figure(4.5):** The ground state energy per spin as a function of the sub-lattice magnetization angle  $\phi$  for different values of  $h$ .

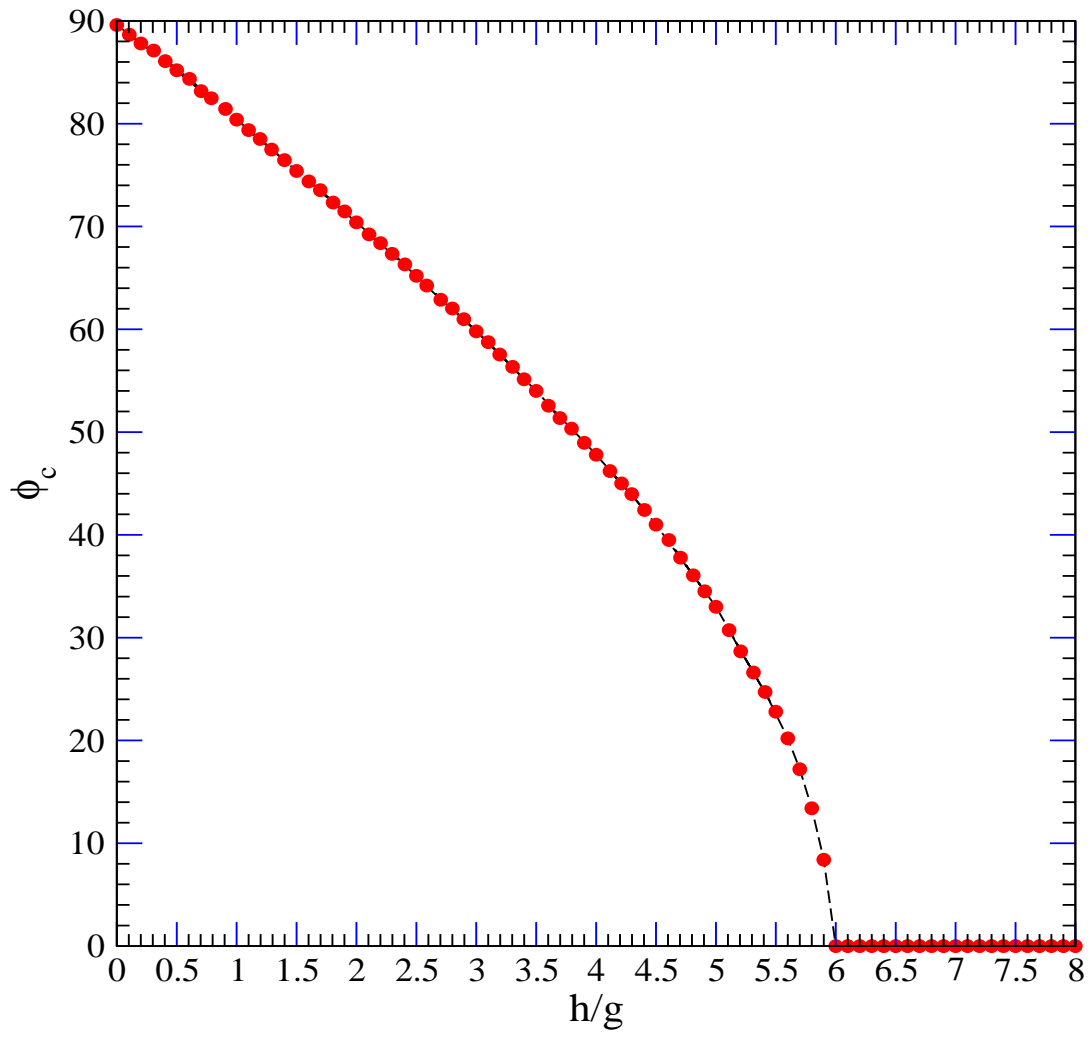


**Figure (4.6):** The critical sub-lattice magnetization angle ( $\phi_c$ ) as a function of The applied magnetic field ( $h/g$ ).

## 4.2 Finite Temperature Properties

The equilibrium phases of interest are the *AF* and *FE* phases. Figure 4.7 show how the order parameters  $M_{AF}$  and  $M_{FE}$ , defined by Equations 4.2 and 4.3 but in terms of the thermally averaged sublattice magnetization, change with both increasing and decreasing the applied field at  $T = 0.10 g$  in an  $N = 104^2$  system. At low temperatures and for ( $h > 6.00 g$ ), the data shown in Figure 4.5 indicate that the ferromagnetic phase is energetically favored ( $\langle M_{AF} \rangle \approx 0$  and  $\langle M_{FE} \rangle \approx 1$ ). At the transition ( $h_R = 5.70 g$ ), the system switches from the ferromagnetic phase to the dipolar antiferromagnetic phase. A similar behavior is observed on increasing the value of the applied field. This implies the existence of a thermally induced reorientation transition between the dipolar phase and the ferromagnetic phase.

Further evidence for the first order phase transition between the two ordered phases is also seen in Figure 4.8, where the behavior of the average sublattice magnetization angle

$$\langle \phi_\alpha \rangle = \arctan \frac{\langle M_\alpha^y \rangle}{\langle M_\alpha^x \rangle} \quad (4.8)$$

is shown as a function of decreasing and increasing the applied field at  $T = 0.10 g$  in an  $N = 104^2$  system. For large values of the applied field ( $h > 6.0 g$ ), Figure 4.8 shows that the spins would all be aligned parallel to the applied field ( $\langle \phi_1 \rangle = \langle \phi_3 \rangle = 0^\circ$  and  $\langle \phi_2 \rangle = \langle \phi_4 \rangle = 360^\circ$ ). At the transition ( $h_R = 5.70 g$ ), the system switches from ferromagnetic phase to an ordered phase in which ( $\langle \phi_1 \rangle = \langle \phi_3 \rangle \cong 30^\circ$ ,  $\langle \phi_2 \rangle = \langle \phi_4 \rangle \cong 330^\circ$ ). As the applied field is

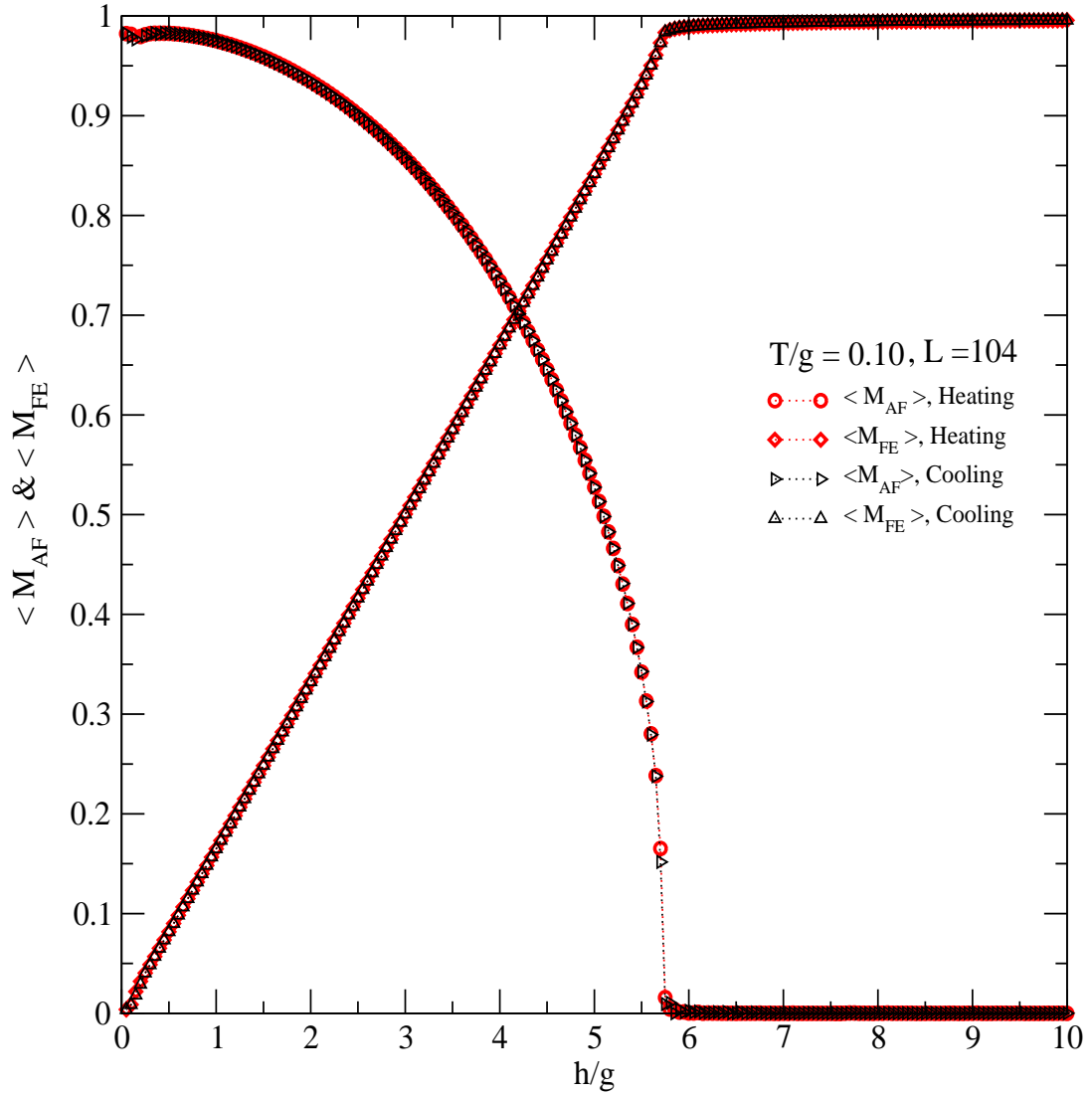


**Figure (4.7):** The two thermally averaged order parameters ( $\langle M_{AF} \rangle$  and  $\langle M_{FE} \rangle$ ) per spin as a function of both decreasing and increasing the applied magnetic field at  $T/g = 0.10$ .

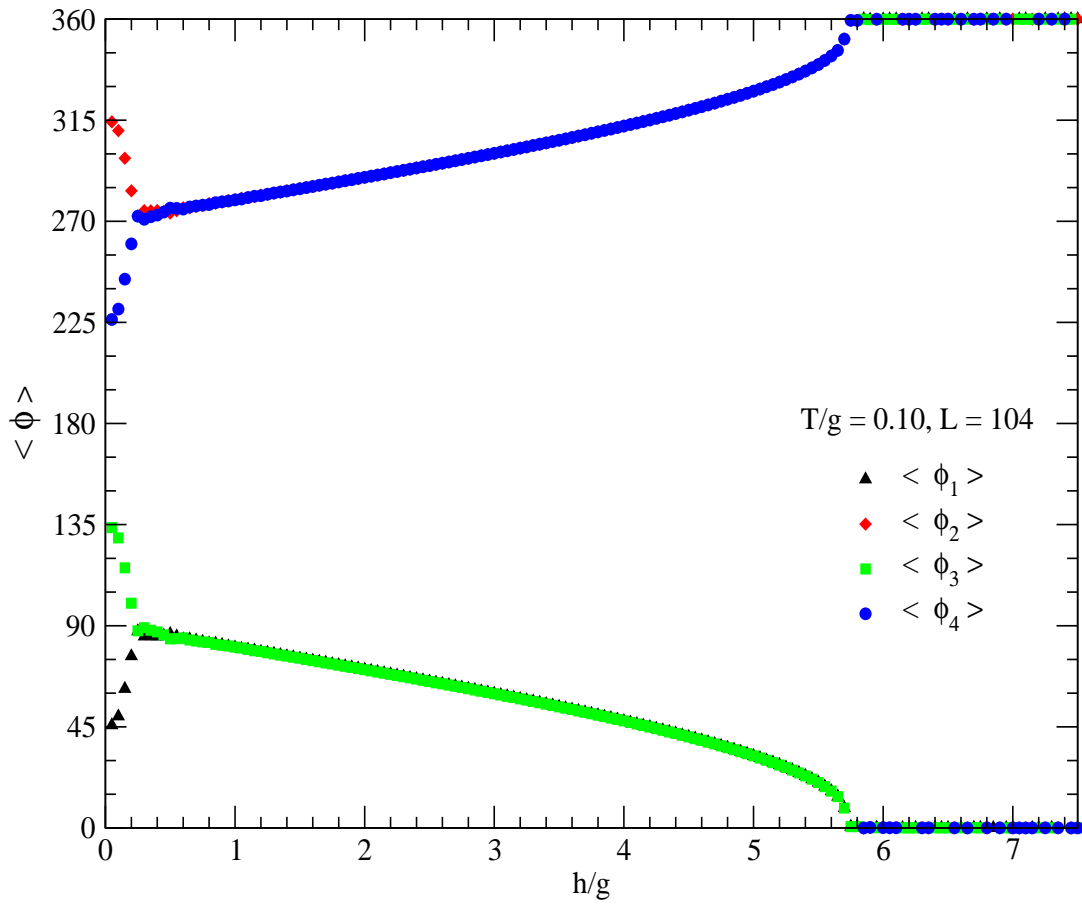


**Figure (4.8):** A plot of  $\langle \phi_\alpha \rangle$ , for each of the sub-lattice magnetization, as a function of both decreasing and increasing the applied magnetic field at  $T/g = 0.10$ .

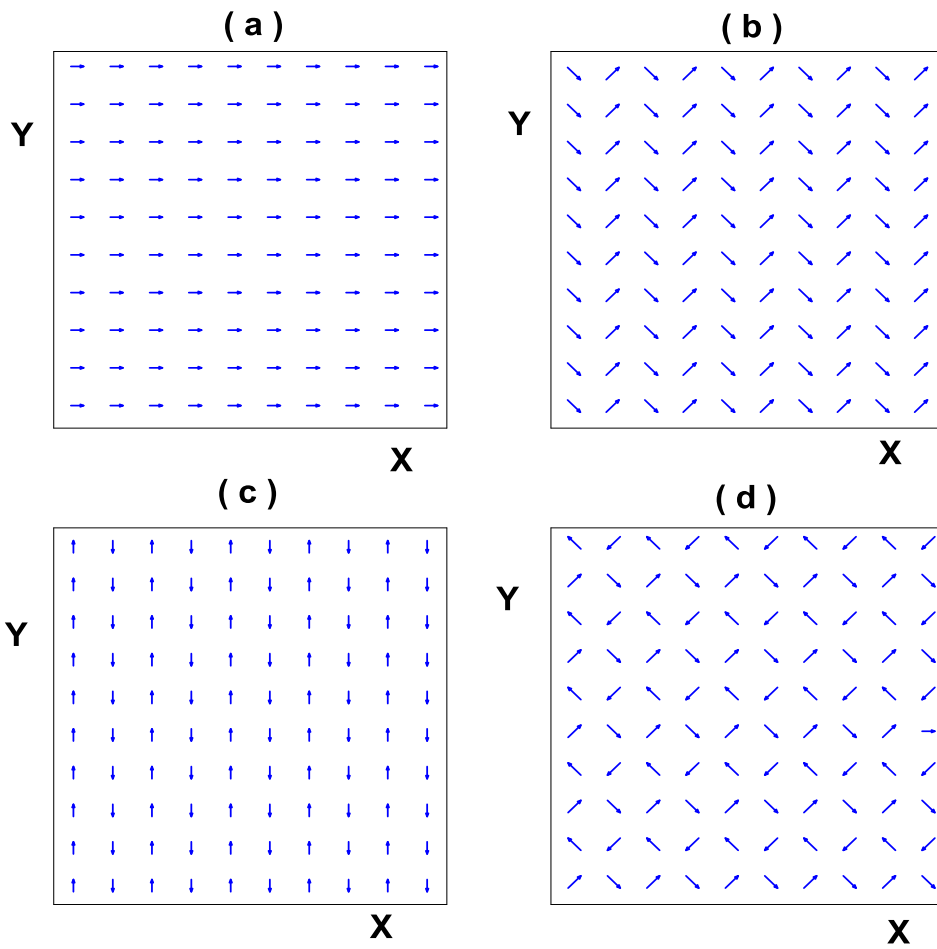


**Figure (4.9):** Snapshots of spin configurations at  $T/g = 0.10$  for (a)  $h/g = 7.00$ , (b)  $h/g = 4.20$ , (c)  $h/g = 0.40$  and (d)  $h/g = 0.05$  in an  $N = 104^2$  system.

decreased, the spin configuration start to turn antiferromagnetically perpendicular to the applied field. At  $h \approx 0.40 g$  the spins become fully ordered antiferromagnetically perpendicular to the field ( $\langle \phi_1 \rangle = \langle \phi_3 \rangle \approx 90^\circ$ ,  $\langle \phi_2 \rangle = \langle \phi_4 \rangle \approx 270^\circ$ ). As the applied field is decreased further, spins in odd numbered columns are rotated clockwise while in even numbered columns are rotated counterclockwise. When the value of the applied field goes to zero, the spins are fully oriented at  $\pm \frac{\pi}{4}$  to the  $x$ -axis ( $\langle \phi_1 \rangle = 45^\circ, \langle \phi_2 \rangle = 315^\circ, \phi_3 = 135^\circ, \phi_4 = 225^\circ$ ). This is consistent with the earlier work for the antiferromagnetic dipolar planar system on a square lattice [106, 108]. Sample spin configurations for  $h/g = 7.00, 4.20, 0.40$  and  $0.05$  are shown in Figure 4.9a, Figure 4.9b, Figure 4.9c, and Figure 4.9d, respectively, at  $T = 0.1g$ . The spin configurations in Figure 4.9 indicate that the symmetry axis is different for different values of the applied field. For  $h = 7g$  Figure 4.9a suggests that the symmetry axis is oriented along the applied field. (i.e., along the  $x$ -axis), while for  $h/g = 0.40$  (Figure 4.9c) and for  $h/g = 0.05$  (Figure 4.9d) the symmetry axis is oriented, respectively, at  $\pm \frac{\pi}{2}$ , and  $\pm \frac{\pi}{4}$  to the  $x$ -axis. It is worth noting that while the data indicate that the transition from the ferromagnetic phase to the dipolar antiferromagnetic is first order, the hysteresis is very small (Figure 4.7), consistent with the discontinuous nature of the transition (Figure 4.8).

At low field, Figure 4.10 shows the thermally averaged order parameters  $\langle M_{AF} \rangle$  and  $\langle M_{FE} \rangle$  as a function of both increasing and decreasing temperature for  $h/g = 1.5$  in an  $N = 104^2$  system. The data plotted in Figure 4.10 show a dipolar antiferromagnetic phase at low

temperature. As the temperature is increased the dipolar order parameter decreases, dropping rapidly at  $T_N = 2.2g$  to indicate the transition from the

ordered dipolar antiferromagnetic phase to the disordered paramagnetic phase. A similar behavior is observed on decreasing temperature.

This indicates a continuous transition (i.e., a second order phase transition) between the low temperature dipolar phase and the paramagnetic phase occurs at  $T_N = 2.20g$ .

The existence of a second order phase transition is also reflected in the behavior of the heat capacity

$$C_H = \frac{\partial E}{\partial T} = \frac{\langle E^2 \rangle - \langle E \rangle^2}{K_B T^2} \quad (4.9)$$

as shown in Figure 4.11. In Figure 4.11 a peak occurs at  $T_N = 2.2g$ . Further evidence for a second order phase transition is also clearly seen in Figure 4.12, where  $\langle M_{AF} \rangle$  and  $\langle M_{FE} \rangle$  are plotted as a function of decreasing temperature for  $h = 1.5g$  in an  $N = 104^2$  and  $N = 64^2$  systems. The data present in Figure 4.12 show sharp transitions as the system size increases, consistent with a second order transition.

At large values of the applied field, Figure 4.13 shows the thermally averaged order parameters  $\langle M_{AF} \rangle$  and  $\langle M_{FE} \rangle$  as a function of both increasing and decreasing temperature for  $h = 8.0g$  in an  $N = 104^2$  system. The data in Figure 4.13 indicate that the system is ferromagnetically ordered at low temperatures. As the temperature is increased, the system

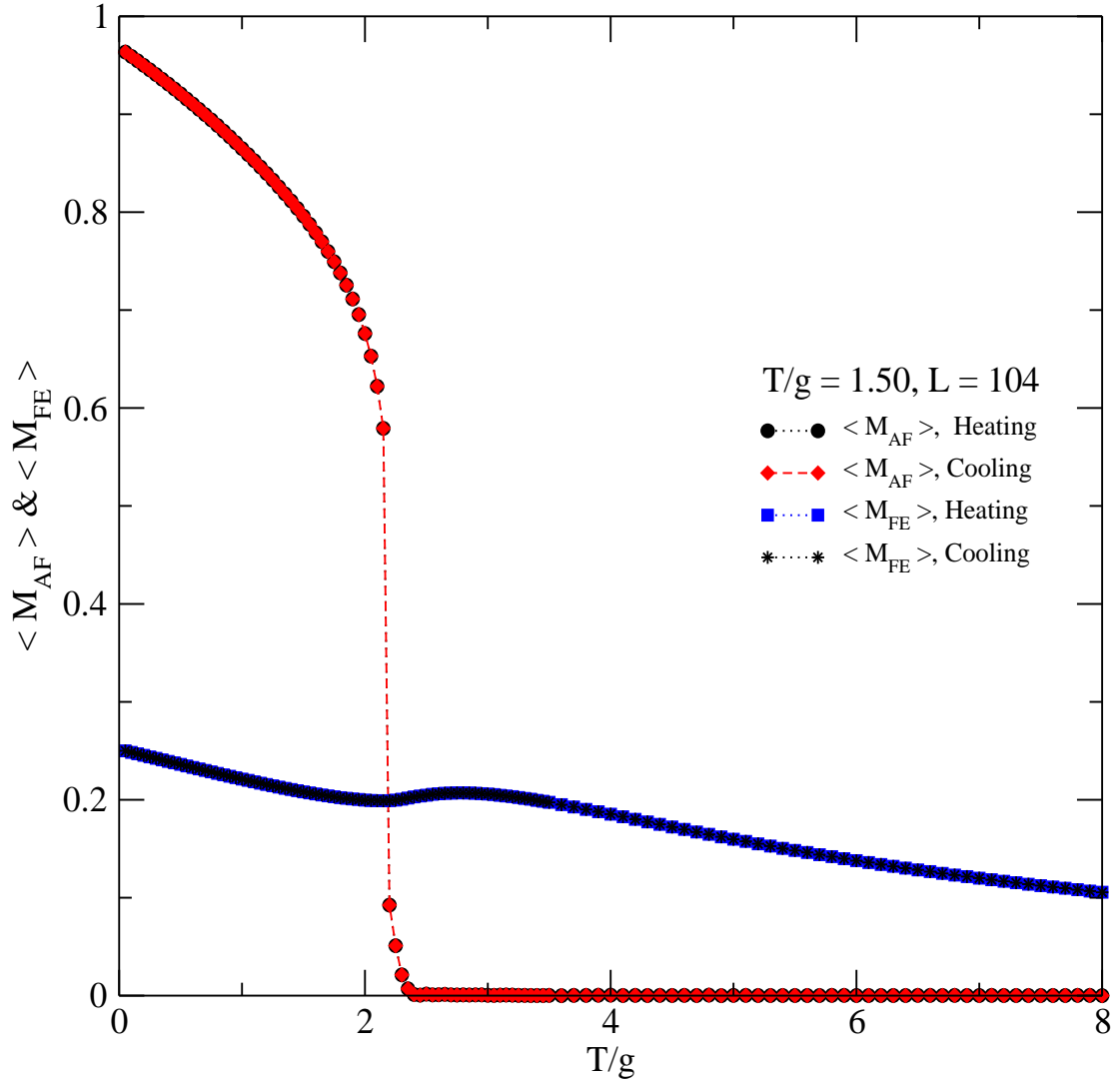


**Figure (4.10):** The two thermally averaged order parameters ( $\langle M_{AF} \rangle$  and  $\langle M_{FE} \rangle$ ) per spin as a function of increasing and decreasing temperature at  $h/g = 1.50$ .

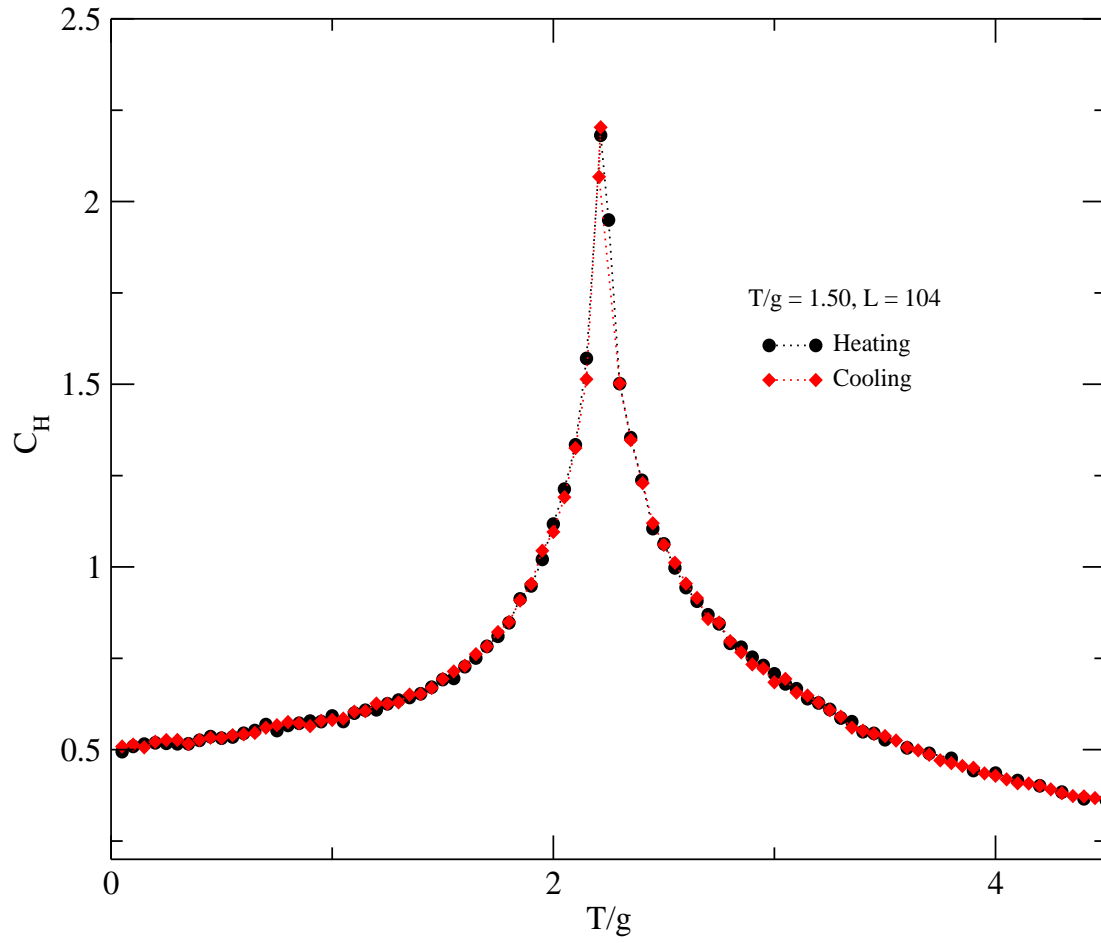


**Figure (4.11):** The specific heat per spin as a function of temperature for heating and cooling the system with  $h/g = 1.50$  in  $N = 104^2$  system.

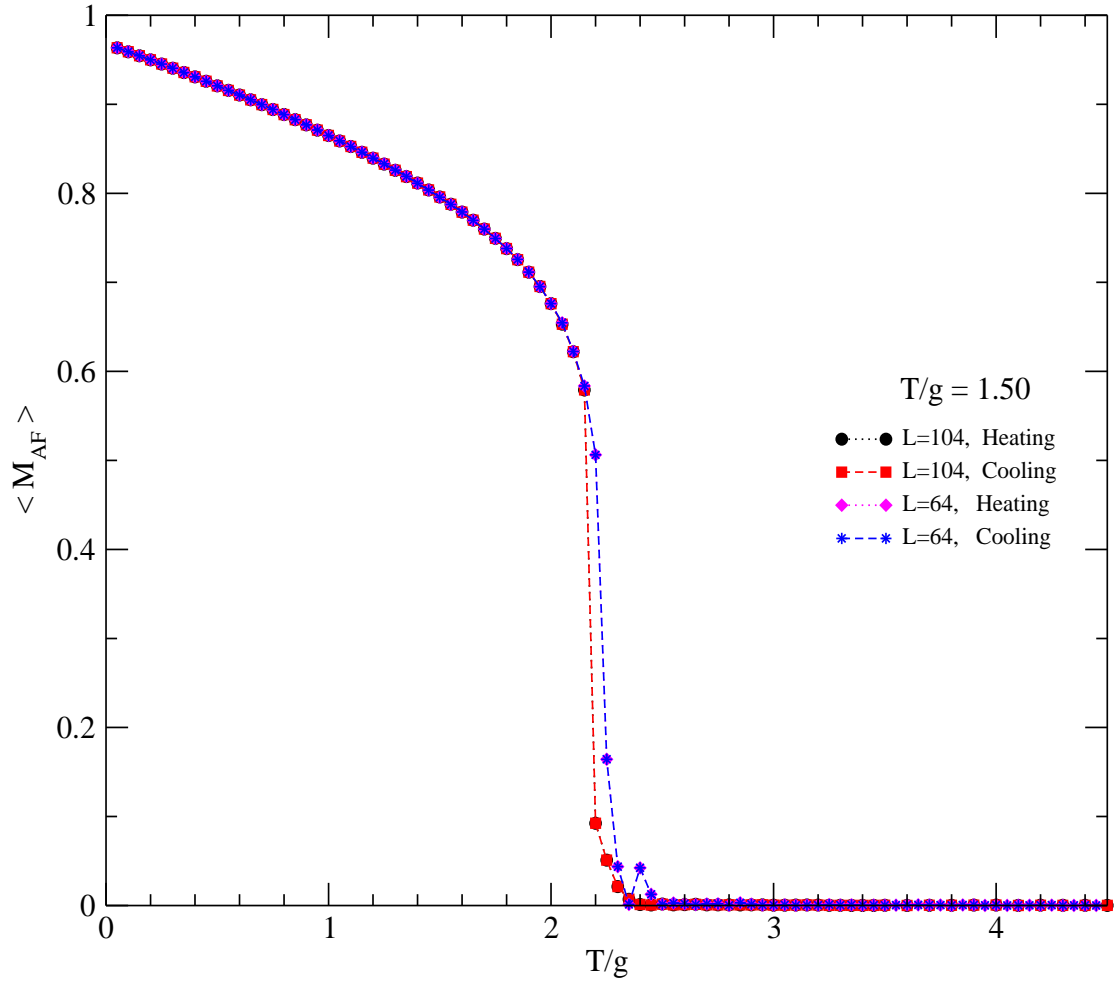


**Figure (4.12):** The thermally averaged order parameters ( $\langle M_{AF} \rangle$ ) per spin as a function of increasing and decreasing temperature at  $h/g = 1.50$  in  $N = 104^2$  and  $N = 64^2$  systems.

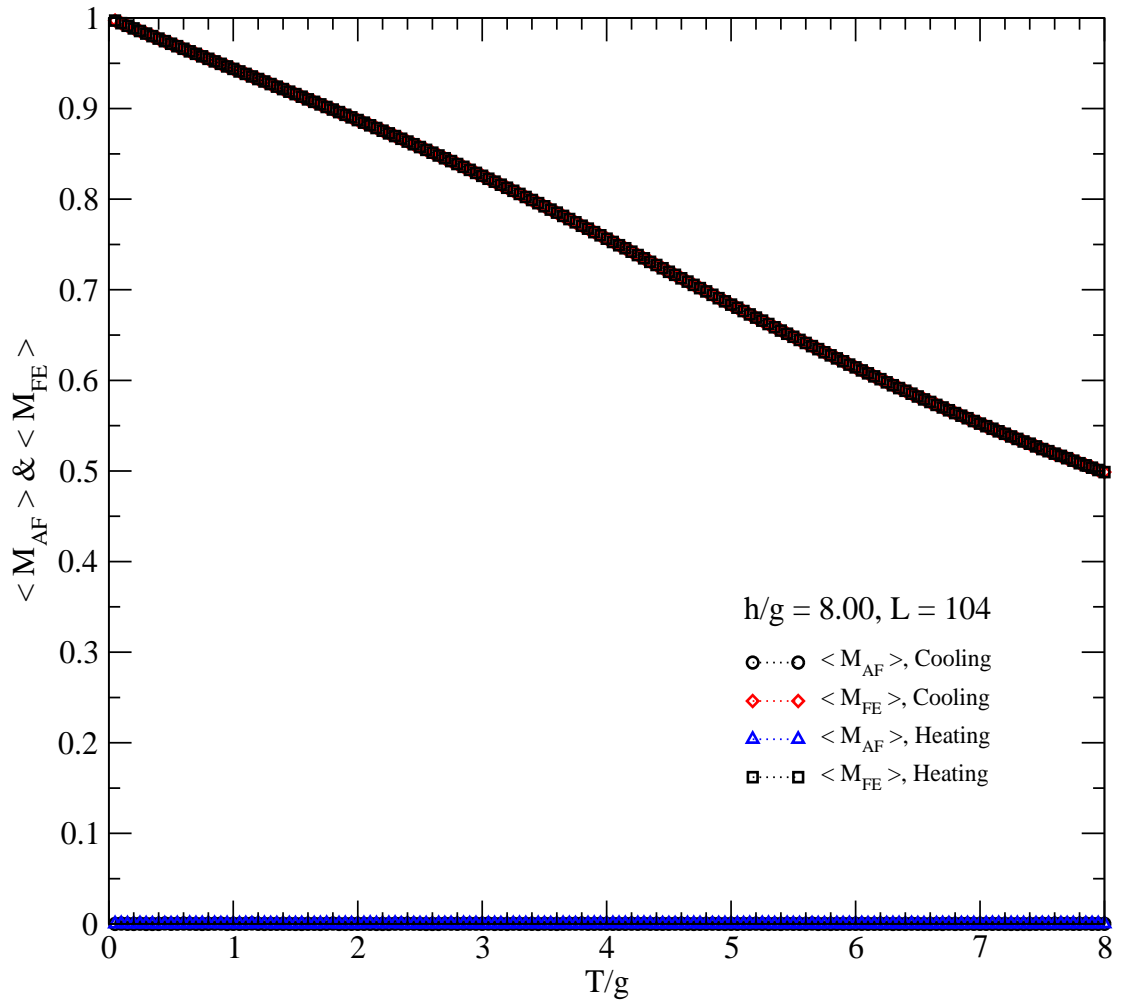


**Figure (4.13):** The thermally averaged order parameters  $\langle MAF \rangle$  and  $\langle MFE \rangle$  as a function of increasing and decreasing temperature for  $h/g = 8.00$  in an  $N = 104^2$  system.

gradually disorders. A similar behavior is observed on decreasing temperature. This agrees with the corresponding heat capacity data shown in Figure 4.14. A rounded peak occurs in the heat capacity data shown in Figures 4.14, which is a remnant of the singularity, is suppressed by the presence of the external magnetic field.

For intermediate value of the applied magnetic field, Figure 4.15 shows  $\langle M_{AF} \rangle$  and  $\langle M_{FE} \rangle$  as a function of both increasing and decreasing temperature for  $h = 4.75g$  in an  $N = 104^2$  system. In Figure 4.15 the data indicate that the two order parameters now behave differently from that shown in Figures 4.7 and 4.10. At low temperature and for this value of  $h$ , the system is in the dipolar antiferromagnetic phase. As the temperature is increased, the thermally averaged dipolar order parameter ( $\langle M_{AF} \rangle$ ) effectively drops to zero while the thermally averaged ferromagnetic order parameter ( $\langle M_{FE} \rangle$ ) increases to a value of  $\sim 0.9$  at the transition temperature  $T_R = 0.85g$ .

As the temperature is increased further, the systems gradually disorders. A similar behavior is observed on decreasing temperature with very small hysteresis. The hysteresis at the transition is shown in more details in Figure 4.16, which shows the two thermally averaged order parameters as a function of increasing and decreasing temperature in the region near the transition temperature. This hysteresis, together with the discontinuous change in the order parameters for both heating and cooling, indicates that the reorientation transition between the dipolar antiferromagnetic phase and the ferromagnetic phase at this value of  $h$  is first order. The reorientation transition shown in Figure 4.15, implies that the competition between the

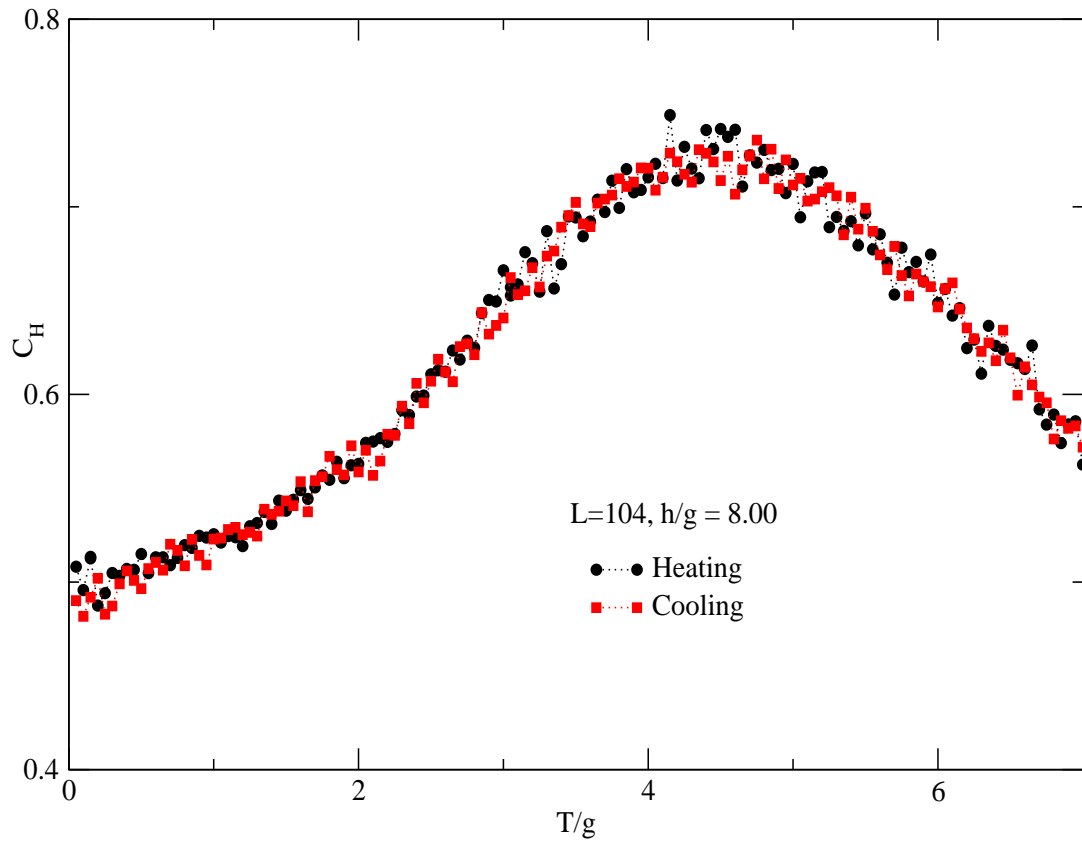


**Figure (4.14):** The heat capacity  $C_H$  as a function of increasing and decreasing Temperature for  $h/g = 8.00$  in an  $N = 1042$  system.

uniform external magnetic field, the dipolar interaction and the antiferromagnetic exchange interaction can give rise to a thermally induced reorientation transition between the two ordered phases.

The temperature dependence of the two thermally averaged order parameters shown in Figure 4.15 is consistent with the heat capacity data shown in Figure 4.17. The heat capacity data plotted in Figure 4.17 show two distinct peaks. The narrow peak corresponding to the reorientation transition between the two ordered phases on heating and cooling, while the broad peak corresponds to a remnant of the singularity due to the presence of the applied magnetic field.

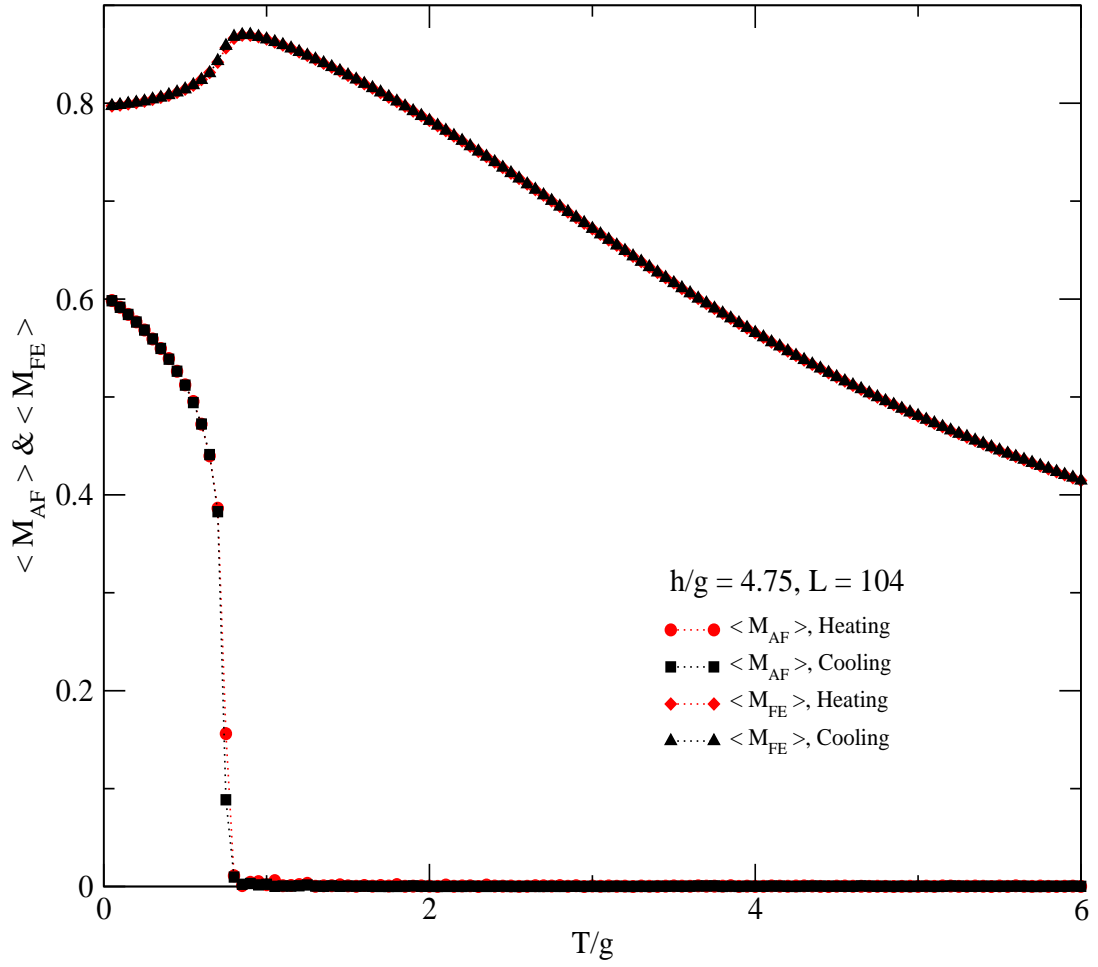


**Figure (4.15):** The thermally averaged order parameters  $\langle M_{AF} \rangle$  and  $\langle M_{FE} \rangle$  as a function of increasing and decreasing temperature for  $h/g = 4.75$  in an  $N = 104^2$  system.

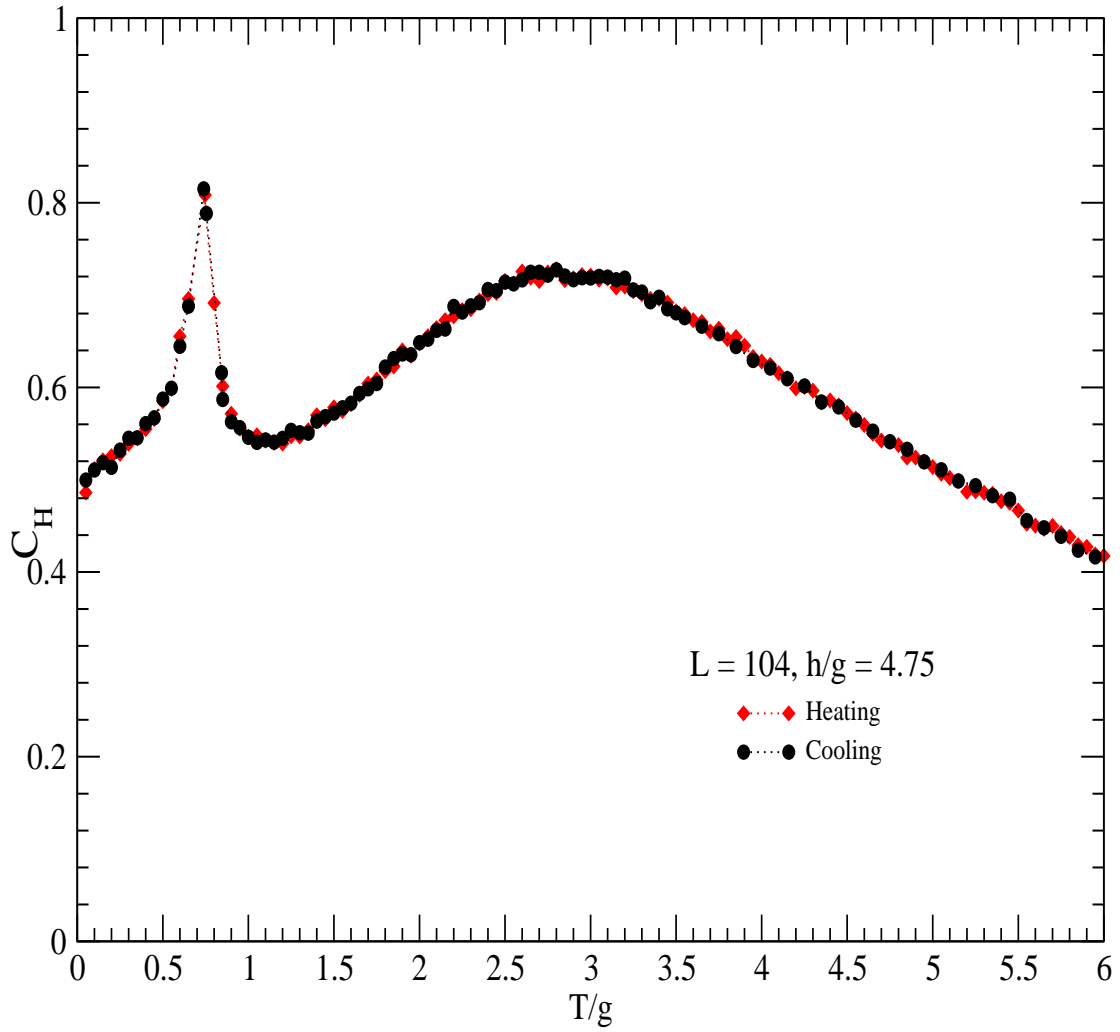


**Figure (4.16):** The thermally averaged order parameters  $\langle M_{AF} \rangle$  and  $\langle M_{FE} \rangle$  as a function of increasing and decreasing temperature for  $h/g = 4.75$  in an  $N = 104^2$  system around the transition point.

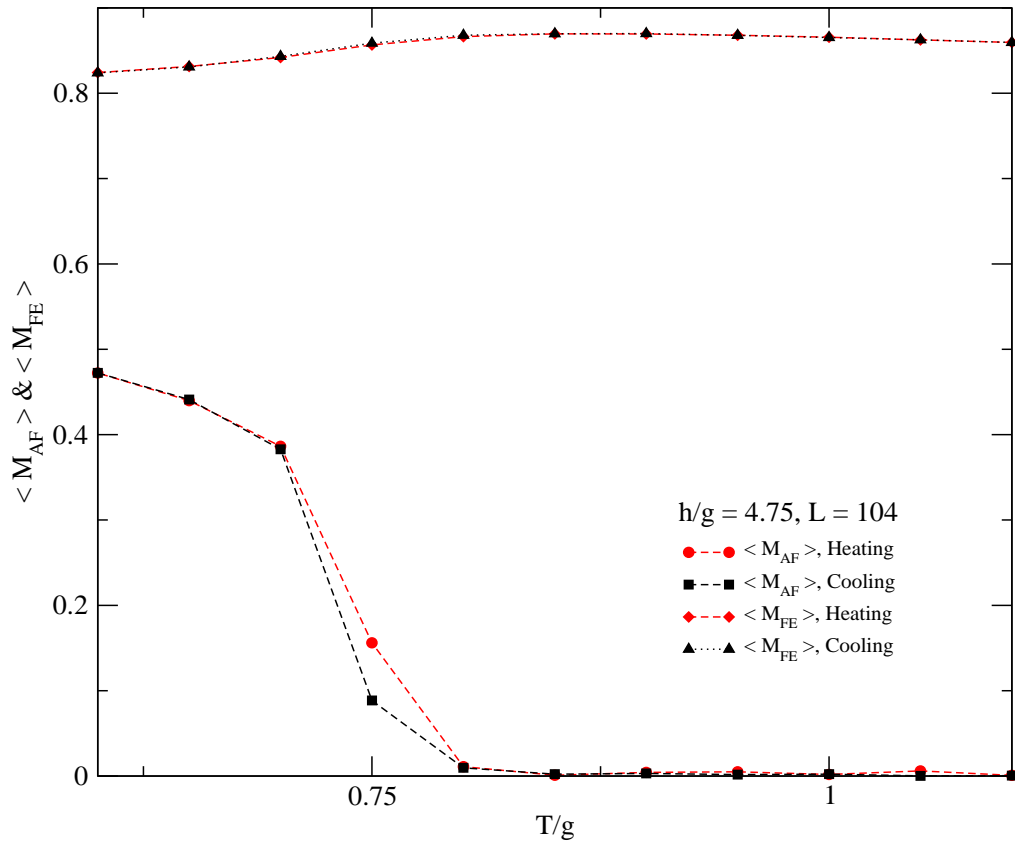


**Figure (4.17):** The heat capacity  $C_H$  as a function of increasing and decreasing temperature in an  $N = 10^4$  system.

### 4.3 The Magnetic Phase Diagram

At finite temperature, the equilibrium phases of the system obtained from Monte Carlo simulations have been presented in the phase diagram shown in Figure 4.18. The phase diagram shows the  $AF$  phase (Region I), in which the ordering corresponds to the dipolar antiferromagnetic phase, the  $FE$  phase (Region II), in which the ordering corresponds to the ferromagnetic phase, and a disordered phase (Region III), in which the ordering corresponds to the paramagnetic phase.

The simulation points separating the two ordered phases (Region I) and (Region II), and the dipolar phase (Region I) from the paramagnetic phase (Region III) are obtained from the points at which the thermally averaged order parameters drop to zero, as well as from the corresponding peak in the magnetic heat capacity. The transition between the two ordered phases (Region I and II) appears to be first order with clear discontinuities in  $\langle \phi \rangle$  [Figures 4.8]. In contrast, the transition between the dipolar antiferromagnetic phase (Region II) and the paramagnetic phase (Region III) appears to be second order with clear size effects [Figures 4.12], continuous in  $\langle M_{AF} \rangle$ , and lack of hysteresis [Figures 4.10]. It is worth noting that in the ferromagnetic phase, there is no transition on heating the system, but the system gradually disorders as the temperature is increased. However, the locus of the rounded peaks in the heat capacity data (due to a remnant of the singularity) is shown as a solid line in the phase diagram. The filled circle point, which indicates the intersection of this locus of maxima with the first-order and second-order transition location of the boundaries, identifies the approximate tricritical point of this system. The approximate location of this tricritical point is ( $T_R = 2.15$  g,  $h_R = 3.00$  g).

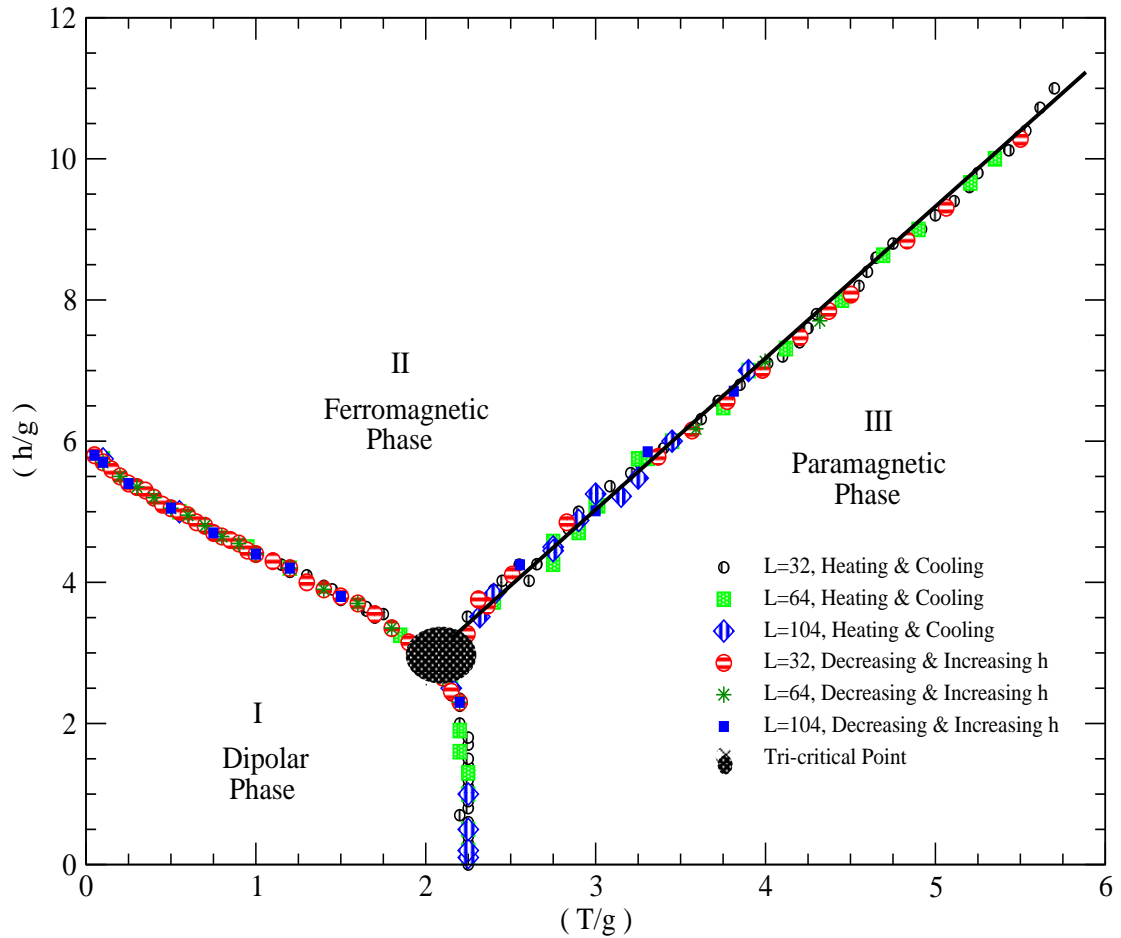


**Figure (4.18):** The magnetic phase diagram for the planar system as a function of the applied magnetic field and temperature in an  $N = 104^2, 64^2, 32^2$  systems. Region I is the dipolar phase, region II is the ferromagnetic phase and region III is the paramagnetic phase. The simulation points between region I and II indicate the line of first-order transition between the dipolar phase and the ferromagnetic phase; whereas the simulation points between region I and region III indicate the line of a second-order transition between the dipolar phase and the paramagnetic phase. The solid line highlights the line where the rounded peaks in the heat capacity data occur due to a remnant of the singularity, which is suppressed by the presence of the applied magnetic field. The filled circle indicates the approximate location of the tri-critical point.

## **Conclusion**

## Conclusion

In this study, the effects of a uniform applied magnetic field on the magnetic properties of the dipolar antiferromagnetic plane rotator system on a square lattice with different sizes ( $N = 32 \times 32$ ,  $64 \times 64$ , and  $104 \times 104$ ) have been studied for both zero and finite temperatures. In particular, the magnetic phase diagram for this system has been determined as a function of both the temperature and applied field using Monte Carlo simulations. As mentioned in Chapter 1, there are many technological and industrial applications for quasi two-dimensional systems, specially, their applications in data storage devices. Since such systems are very sensitive to the action of an external magnetic field, it is a better to understand the effects of a uniform applied magnetic field on the nature and stability of these systems.

In the current work, a uniform external magnetic field is applied parallel to the axis of the square lattice and the exchange interaction parameter  $J$  is assumed to be antiferromagnetic and fixed at  $-1.20$  relative to the dipolar parameter  $g$ . At zero temperature and for low values of a uniform applied field the ground state energy calculations show that the spins are in a dipolar antiferromagnetic phase ( $AF_1$  phase) perpendicular to the field. As the applied field is increased, the dipolar order parameter decreases continuously until the system undergoes a first order transition to

the ferromagnetic phase at  $h_o = 6.00$  g. At low temperature, and for zero applied field, however, Monte Carlo simulations show a dipolar antiferromagnetic phase in which the spins are oriented at  $\pm \frac{\pi}{4}$  to the  $x$ -axis ( $AF_2$  phase). This result is consistent with what Abu-Labdeh *et al* found for the dipolar antiferromagnetic plane rotator system on a square lattice [98]. As the applied field is increased, the spins rotate continuously until the system becomes in the  $AF_1$  phase perpendicular to the field. Further increase in the applied field, the spins rotate continuously until a first order transition to the ferromagnetic phase occurs.

At small values of the applied field and for low temperatures, Monte Carlo results show a finite dipolar order parameter. As the temperature is increased the dipolar order parameter decreases continuously until the system undergoes a second order transition to the disordered phase (paramagnetic phase). On the other hand, Monte Carlo simulations for large values of the applied field show a finite ferromagnetic order parameter in which the spins are aligned along the applied field. As the temperature is increased, the ferromagnetic order parameter gradually decreases. For intermediate values of the applied field, there exists a range around  $h_o = 6.00$  g for which the system undergoes a first order reorientation transition from the dipolar phase to the ferromagnetic phase with increasing temperature. As the temperature is further increased the system gradually disorders. These results are summarized in the phase diagram shown in Figure 4.18.

## **References**

## References

- [1] Wolf S A, Awschalom D D, Buhrman R A, Daughton J M, von olnar S, Roukes M L, Chtchelkanova A Y, and Treger D M. **Spintronics: A spin -based electronics vision for the future**, *Science*, **294**:1488-1495, 2001 .
- [2] Freeman M R, and Choi B C. **Advances in magnetic microscopy**, *Science*, **294**: 1484 – 1488, 2001.
- [3] Prutton M. *Introduction to surface physics*, Clarendon Press, Oxford, 1994 .
- [4] Jones T L, and Venus D. **Structural and magnetic characterization of thin iron films on a tungsten (001) substrate**, *Surface Science*, **302**:126 – 140, 1994
- [5] Pappas D P, Kamper K -P, and Hopster H. **Reversible transition between perpendicular and in-plane magnetization in ultrathin films**, *Physical Review Letters*, **64** (26): 3179-3182, 1990.
- [6] Allenspatch R, and Bischof A. **Magnetization direction switching in Fe/Cu(100) epitaxial films: Temperature and thicknes dependence**, *Physical Review Letters*, **69** (23):3385-3388, 1992 .
- [7] Qiu Z Q , Pearson J, and Bader S D. **Asymmetry of the spin reorientation transistion in ultrathin Fe films and wedges grown on Ag(100)**, *Physical Review Letters*, **70**(7):1006-1009, 1993.

- [8] Berger A, and Hopster H. **Magnetization reversal properties near the reorientation phase transition of ultrathin Fe/Ag(100) films**, *Journal of Applied Physics*, **79**(8):5619-5621,1996 .
- [9] Allenspatch R, Stampanoni M, and Bischof A. **Magnetic domains in thin epitaxial Co/Au(111) films**, *Physical Review Letters*, **65**(26):3344-3347,1990 .
- [10] Speckmann M, Oepen H P, and Ibach H. **Magnetic domain structure in ultrathin Co/Au(111): On the influence of film morphology**, *Physical Review Letters*, **75**(10):2035-2038,1995.
- [11] Liu C, and Bader S D. **Perpendicular surface magnetic anisotropy in ultrathin epitaxial Fe films**, *Journal of Vacuum Science and Technology A*, **8** (3):2727-2731,1990.
- [12] Schulz B, and Baberschke K. **Crossover from in-plane to perpendicular magnetization in ultrathin Ni/Cu(001) films**, *Physical Review B*, **50** (18):13467-13471,1994.
- [13] Baberschke K. **The magnetism of nickel monolayers**, *Applied Physics A*, **62**:417-427,1996.
- [14] Farle M, Platow W, Anisimov A N, Schulz B, and Baberschke K. **The temperature dependence of magnetic anisotropy in ultrathin films**, *Journal of Magnetism and Magnetic Materials*, **165**:74-77, 1997.

- [15] Roland C, and Grant M. Lack of self averaging, **multi scaling, and i/f noise in the kinetics of domain growth**, *Physical Review Letters*, **63** (5):551- 554,1989.
- [16] Roland C, and Desai R C. **Kinetics of quenched systems with long-range repulsive interactions**, *Physical Review B*, **42**(10):6658-6669,1990.
- [17] Sagui C, and Desai R C. **Kinetics of phase separation in two-dimensional systems with competing interactions**, *Physical Review E*, **49**(3):2225- 2244,1994.
- [18] Kortright J B, Awschalom D D, Stohr J, Bader S D, Idzerda Y U, Parkin S S P, Ivan Schuller K, and Siegmann H C. **Research frontiers in magnetic materials at soft X-ray synchrotron radiation facilities**, *Journal of Magnetism and Magnetic Materials*, **207**:7-44,1999.
- [19] Prinz G A. **Magnetoelectronics**, *Science*, **282**:1660-1663, (1998).
- [20] Richter H J. **Recent advances in the recording physics of thin-film media**. *Journal of Physics D: Applied Physics*, **32**(21): R127-R168, 1999.
- [21] Heinrich B, and Cochran J F. **Ultrathin metallic magnetic films: Magnetic anisotropies and exchange interactions**. *Advances in Physics*, **42** (5):523-639, 1993.

- [22] Bland J A C, and Heinrich B. **Ultrathin Magnetic Films, volume I, II.** *Springer-Verlag*, Berlin, 1994.
- [23] Nogues J, and Schuller I K. **Exchange bias.** *Journal of Magnetism and Magnetic Materials*, **192**:203-232, 1999.
- [24] Dieny B, Speriosu V S, Parkin S S P, Gurney B A, Wilhoit D R, and Mauri D. **Giant magnetoresistance in soft ferromagnetic multilayers.** *Physical Review B*, **43** (1):1297-1300, 1991.
- [25] Parkin S S P, Roche K P, Samant M G, Rice P M, Beyers R B, Scheuerlein R E, O'Sullivan E J, Brown S L, Bucchignano J, Abraham D W, Rooks Y L, M, Trouilloud P L, Wanner R A, and Gallagher W. J. **Exchange-biased Magnetic tunnel junctions and application to nonvolatile magnetic random access memory (invited),** *Journal of Applied Physics*, **85**(8):5828- 5583, 1999.
- [26] Tsang C, Tsann Lin R E F, Heim D E, Speriosu V S, Gurney B A, and Williams M L. **Design, fabrication, and testing of spin-valve read heads for high density recording,** *IEEE Transactions on Magnetics*, **30**(6):3801-3806,1994.
- [27] Parkin S S P, and Mauri D. **Spin engineering: Direct determination of the Ruderman-Kittle-Kasuya-Yosida far-field range function in ruthenium,** *Physical Review B*, **44**(13):7131-7134,1991.

- [28] Daughton J, Brown J, Chen E, Beech R, Pohm A, and Kude W. **Magnetic field sensors using GMR multilayer**, *IEEE Transactions on Magnetics*, **30**(6):4608-4610,1994.
- [29] Borchers J A, Erwin R W, Berry S D, Lind D M, Ankner J F, Lochner E, Shaw K A, and Hilton D. **Long-range magnetic order in  $\text{Fe}_3\text{O}_4/\text{NiO}$  super lattices**, *Physical Review B*, **51**(13):8276-8286,1995.
- [30] Spanke D, Solinus V, Knabben D, Hillebrecht F U, Ciccacci F, Gregoratti L, and Marsi M. **Evidence for in-plane antiferromagnetic domains in ultrathin NiO films**, *Physical Review B*, **58**(9):5201-5204,1998.
- [31] Baruchel J. **X-ray and neutron topographical of magnetic materials**, *Physica B*, **192**:79-93,1993.
- [32] Stohr J, Sholl A, Luning J, Scheinfein M R, Padmore H A, and White R L. **Images of the antiferromagnetic structure of a NiO surface by means of X-ray magnetic linear dichroism spectromicroscopy**, *Physical Review Letters*, **83**(9):1862-1865,1999.
- [33] Sholl A, Stohr J, Luning J, Seo J W, Fempeyryne J, Siegwart H, Locquet J P, Nolting F, Anders S, Fullerton E E, Scheinfein M R, and Padmore H A, **Observations of antiferromagnetic domains of epitaxial thin films**, *Science*, **287**:1014-1016,2000.

- [34] De' Bell K, and Whitehead J P. **The dipole-dipole contribution to the magnetic propagator in the  $\text{REBa}_2\text{Cu}_3\text{O}_{7-\delta}$  compounds**, *Journal of Physics : Condensed Matter*, 3: 2431 - 2439, 1991.
- [35] De' Bell K, MacIsaac A B, and Whitehead J P. **Dipolar effects in magnetic thin films and quasi-two-dimensional systems**, *Review of Modern Physics*, **72**(1):225- 257,2000.
- [36] Lynn J W, Li W-H, Li Q, Ku H C, Yang H D, and Shelton R N. **Magnetic fluctuations and two-dimensional ordering in  $\text{ErBa}_2\text{Cu}_3\text{O}_7$** , *Physical Review B*, **36**(4):2374-2377,1987.
- [37] Lynn J W. **High Temperature superconductivity**, *Springer-Verlag*, NewYork,1990.
- [38] Clinton T W, and Lynn J W. **Magnetic ordering of Er in powder and single crystals of  $\text{ErBa}_2\text{Cu}_3\text{O}_7$** , *Physica C*, **174**:487-490,1991.
- [39] Lynn J W. **Two-dimensional behavior of the rare earth ordering in oxide superconductors**, *Journal of Alloys and Compounds*, **181**,1992.
- [40] Clinton T W, Lynn J W, Liu J Z, Jia Y X, Goodwin T J, Shelton R N, Lee B W, Buchgeister M, Maple M B, and Peng J L. **Effects of oxygen on the magnetic order of the rare-earth ions in  $\text{RBa}_2\text{Cu}_3\text{O}_{6+x}$  (R=Dy,Er,Nd)**, *Physical Review B*, **51**(21):15429-15447,1995.

- [41] Skanthakumar S, and Lynn J W. **Spin dynamics of Er<sup>3+</sup> ions in RBa<sub>2</sub>Cu<sub>3</sub>O<sub>7-δ</sub>**, *Journal of Applied Physics*, **81**(8):4934-4936,1997.
- [42] Tarascon J M, McKinnon W R, Greene L H, Hull G W, and Vogel E M. **Oxygen and rare earth doping of the 90-K superconducting perovskite YBa<sub>2</sub>Cu<sub>3</sub>O<sub>7-x</sub>**, *Physical Review B*, **36**(1):226-234,1987.
- [43] Knobel M, Sampaio L C, Sinnecker E H C P, Vargas P, and Altbir D. **Dipolar magnetic interactions among magnetic microwires**, *Journal of Magnetism and Magnetic Materials*, **249**:60-72,2002.
- [44] Sampaio L C, Hyndman R, de Menezes F S, Jamet J P, Meyer P, Gierak J, Chappert C, Mathet V, and Ferre J. **Power-law relaxation decay in two dimensional arrays of magnetic dots interacting by long-range dipole- dipole interactions**, *Physical Review B*, **64**(18):4440(1)-4440(7),2001.
- [45] Sampaio L C, Sinnecker E H C P, Cernicchiaro G R C, Knobel M, V´azquez M, and Vel´azquez J. **Magnetic microwires as macrospins in a long range dipole-dipole interaction**, *Physical Review B*, **61**(13),8976-8983,2000.
- [46] Knobel M, Sampaio L C, Sinnecker E H C P, Vargas P, and Altbir D. **Dipolar magnetic interactions among magnetic microwires**, *Journal of Magnetism and Magnetic Materials*, **249**, 60,2002.

- [47] Hertel R. **Numerical studies of demagnetizing effects in triangular ring arrays**, *Journal of Applied Physics*, **90**: 5752, 2001.
- [48] Clime L, Ciureanu P, and Yelon A. **Magnetostatic interactions in dense nanowire arrays**, *Journal of Magnetism and Magnetic Materials*, **297**, 60, 2006.
- [49] Bahiana M, Amaral F S, Allende S, and Altbir D. **Reversal modes in arrays of interacting magnetic Ni nanowires: Monte Carlo simulations and scaling technique**, *Physical Review B* **74**, (17)4412, 2006.
- [50] Sorop T G, Untiedt C, Luis F, Kroll M, Rasa M, and de Jongh L J. *Physical Review B* **67**, 014402, 2003.
- [51] Cowburn R P, Adeyeye A O, and Welland M E. **Controlling magnetic ordering in coupled nanomagnet arrays**, *New Journal of Physics*, **1**(6):19, 1999.
- [52] Cowburn R P. **Property variation with shape in magnetic nanoelements**, *Journal of Physics D: Applied Physics*, **33**:R11-R16, 2000.
- [53] Giersig M and Hilgendorf M. **The preparation of ordered colloidal magnetic particles by magnetophoretic deposition**, *Journal of Physics D: Applied Physics*, **32**: L111-L113, 1999.

- [54] Hyndman R, Mougén A, Sampaio L C, Ferre J, Jamet J P, Meyer P, Mathet V, Chappert C, Mailly D, and Gierak J. **Magnetization reversal in weakly coupled magnetic patterns**, *Journal of Magnetism and Magnetic Materials*, **240**:34-36:1467-1469,2002.
- [55] Sinnecker E H C P, de Meezes F S, Sampaio L C, Konbel M, and Vazquez M. **Tailoring coercivity in an array of glass-coated microwires**, *Journal of Physics D* , **29**: 226-236, 2001.
- [56] Vazquez M, and Hernando A. **A soft magnetic wire for sensor applications**, *Journal of Physics D* , **29**: 939-949, 1996.
- [57] Chiriac H and Ovari T A. **Amorphous glass-covered magnetic wires: preparation, properties, applications**,*Physical Review B*, **40**: 333- 407, 1996.
- [58] Sampaio L C, Sinnecker E H C P, Cernicchiaro G R C, Knobel M, Vázquez M, and Velázquez J. **Magnetic microwires as macrospins in a long range dipole-dipole interaction**, *Physical Review B*, **61**(13),8976-8983, 2000.
- [59] Hehen M, Ounadjela K, Ferre R, Grange W, and Rousseaux F. **Reorientational magnetic transition in mesoscopic cobalt dots**, *Applied Physics Letters*, **71**(19):2833-2835, 1997.
- [60] Prinz G. **Magnetoelectronics**, *Science* **282**, 1660, 1998.

- [61] Cowburn R P. **Property variation with shape in magnetic nanoelements**, *Journal of Physics D: Applied Physics*, **33**:R11-R16, 2000.
- [62] Escrig J, Landeros P, Altbir D, Vogel E E, and Vargas P. **Phase diagrams of magnetic nanotubes**, *Journal of Magnetizm and Magnetic Materials*, **308**, 233-237,2007.
- [63] Escrig J, Landeros P, Altbir D, Bahiana M, and d'Albuquerque e Castro J. *Applied Physics Letteres*, **89**, 132501, 2006
- [64] Nielsch K, Wehrspohn R B, Barthel J, Kirschner J, Fischer S F, Kronmuller H, Schweinbock T, Weiss D, and Gosele U. *Journal of Magnetism and Magnetic Materials*, **291**, 234-240,2002.
- [65] Nielsch K, Wehrspohn R B, Barthel J, Kirschner J, Gosele U, Fischer S F, and Kronmuller H. *Applied Physics Letteres*, **79**, 1360, 2001.
- [66] V´azquez M, Nielsch K, Vargas P, Vel´azquez J, Navas D, Pirota K, Hern´andez- V´elez M, Vogel E, Cat´es J, Wehrspohn R B, and Gosele U, *Physica B*, **343**, 395, 2004.
- [67] V´azquez M, Pirota K, Torrej´on J, Navas D, and Hern´andez-V´elez M, *Journal of Applied Physics*, **294**, 174, 2005.
- [68] Masuda H and Fukuda K. *Science*, **268**, 1466, 1995.
- [69] Skomski R, Zeng H, Zheng M, and Sellmyer D J, *Physical Review B*, **62**, 3900, 2000.

- [70] Asenjo A, Jafaar M, Navas D, and V´azquez M. *Journal of Applied Physics*, 100, 023909, 2006.
- [71] Jensen P J and Bennemann K H, *Surface Science Reports*, **61**:129, 2007.
- [72] De’Bell K, MacIsaac A B, and Whitehead J P. **Dipolar effects in magnetic thin films and quasi-two dimensional systems**, *Review of Modern Physics*, **72** : 225, 2000.
- [73] Abu-Labdeh A M, and MacIsaac A B. **Effects of a Uniform External Magnetic Field on the Magnetic Properties of a Pure Dipolar Planar System**, *Physical Review B*, **73**, 094412, 2006.
- [74] Rapini M, Dias R A, and Costa B V. **Phase transition in ultrathin magnetic films with long-range interactions: Monte Carlo simulation of the anisotropic Heisenberg model**, , *Physical Review B* ,**75**, 014425, 2007
- [75] Gatteschi D, Caneschi A, Pardi L, and Sassoli R, *Science*, **265**, 1054, 1994.
- [76] Merzln N D and Wagner H. **Absence of ferromagnetism or antiferro- magnetism in one- or two-dimensional isotropic Heisenberg models**, *Physical Review Letters*, **17**:1133-6, 1966.
- [77] Bloch F. **Zur theorie des ferromagnetismus**, *Zeitschrift fur Physik*, **49**: 206-219,1928.

- [78] Belobrove P I, Gekht R S, and Ignatchenko V A. **Ground state in systems with dipole interaction**, *Soviet Physics JETP*, **57**(3):636-642, 1983.
- [79] Luttinger J M, and Tisza L. **Theory of dipole interaction in crystals**, *Physical Review*, **70** (11-12): 954 - 964, 1946.
- [80] Zimmerman G O, Ibrahim A K, and Wu F Y. **Planar classical dipolar system on a honeycomb lattice**, *Physical Review B*, (374):2059-2065, 1988.
- [81] Henley C L. **Ground-state selection in fcc vector antiferromagnets**, *Journal of Applied Physics*, **61**(8):3962-3964, 1987.
- [82] Henley C L. **Ordering due to disorder in a frustrated vector antiferromagnet**, *Physical Review Letters*, **62**(17):2056-2059, 1989.
- [83] Parakash S and Henley C L. **Ordering due to disorder in dipolar magnets on two-dimensional lattices**, *Physical Review B*, **42**(10):6574-6589, 1990.
- [84] DeBell K, MacIsaac A B, Booth I N, and Whitehead J B, **Dipolar-induced planar anisotropy in ultrathin magnetic films**, *Physical Review B*, **55**(22):15108-15118, 1997.
- [85] Rastelli E, Carbognani A, Regina S, and Tassi A. **Order by thermal disorder in 2D planar rotator model with dipolar interaction**, *The European Physical Journal B*, **9**:641-649, 1999.

- [86] Rasteili E, Regina S, Tassi A, and Carbognani A. **Long-range isotropic and dipolar spin-spin interactions in the square planar rotator model**, *Physical Review B*, **65**(9):094412(1)-094412(16), 2002.
- [87] Abu-Labdeh A M, Chafe N P, Whitehead J P, De'Bell K, and MacIsaac A B. **Phase behaviour of the antiferromagnetic plane rotator model**, *Journal of Physics: Condensed Matter*, 147155-7163, 2002.
- [88] Abu-Labdeh A M and MacIsaac A B. **Effects of a uniform external magnetic field on the magnetic properties of a pure dipolar planar system**, *Physical Review B*, **73**, 094412-094420, 2006.
- [89] Weber W, Back C h, Bischof A, Pescia D, and Allenspach R., **Magnetic switching in cobalt films by adsorption of copper**, *Nature (London)*, 374,788-790, 1995.
- [90] MacIsaac A B. **Monte Carlo study of the two-dimensional Ising model**. *Masters thesis*, Memorial University, 1992.
- [91] Fujiki N M, De'Bell K, and Geeldart D J W. **Lattice sums for dipolar systems**. *Physical Review B*, **36**(16):8512-8516, 1987.
- [92] Landau D P, and Binder K. *A Guide to Monte Carlo Simulations in Statistical Physics*, Cambridge University Press, 2000.
- [93] Metropolis N, and Ulam S. **The Monte Carlo method**, *Journal of the American Statistical Association*, **44** 335, 1949.

- [94] Novotny M A. **Monte Carlo with absorbing Markov chains: fast local algorithm for slow dynamics**, *Physical Review Letters*. **74** 1 (1995);Erratum, 75 1424 (1995);eprint: arXiv: cond-mat/9411081,1994.
- [95] Bortz A B, Kalos M H, and Lebowitz J L. **A new algorithm for Monte Carlo simulation of Ising spin systems**, *Journal of Computational Physics*, 1710,1975.
- [96] Berg B A, and Neuhaus T. **Multicanonical ensemble: a new approach to simulation of first order phase transition**, *Physical Review Letters*, 68 9, 1992.
- [97] Metropolis N, Rosenbluth A W, Rosenbluth M N, Teller A H, and Teller E. **Equation of state calculation by fast computing machine**, *Journal of Chemical Physics*. 21 1087, 1953.
- [98] Abu-Labdeh A M, Chafe N P, Whitehead J P, De'Bell K, and MacIsaac A B. *Journal of Physics: Condensed Matter*,147155-7163, 2002.
- [99] Simizu S, Bellesis G H, Lukin J, Friedberg S A, Lessure H S, Fire S M, and Greenblatt M. *Physical Review B*, **39**,9099, 1989.
- [100] MacIsaac A B. **Monte Carlo study of the two-dimensional dipolar Ising model**. *Master's thesis*, Memorial University, 1992.
- [101] MacIsaacAB. **The magnetic properties of a model two-dimensional dipolar thin film**. *PHD thesis*, Memorial University, 1997.
- [102] Abu-Labdeh A M. **Monte Carlo Simulations for Classical Two- dimensional Dipolar Antiferromagnetic Systems on a Square Lattice**. *PHD thesis*, Memorial University, 2004.

- [103] Belbrove P I, Gekht R S, and Ignatchenko V A. **Ground state in systems with dipolar interaction.** *Soviet Physics JETP*, 57(3):636-642, 1983.
- [104] Zimmerman G O, Ibrahim A K, and Wu F Y. **Planar classical dipolar system on a honeycomb lattice.** *Physical Review B*, 37(4):2059-2065, 1988.
- [105] DeBell K, MacIsaac A B, Booth I N, and Whitehead J B. **Dipolar induced planar anisotropy in ultrathin magnetic films.** *Physical Review B*, 55(22):15108-15118, 1997.
- [106] Abu-Labdeh A M, Chafe N P, Whitehead J P, De'Bell K, and MacIsaac A B. **Phase behaviour of the antiferromagnetic plane rotator model,** *Journal of Physics: Condensed Matter*, 147155-7163, 2002.
- [107] Parakash S. and Henley C L. Ordering **due to disorder in dipolar magnets on two-dimensional lattices.** *Physical Review B*, 42(10):6574-6589, 1990.
- [108] Rasteili E, Regina S, Tassi A, and Carbognani A. **Long-range isotropic and dipolar spin-spin interactions in the square planar rotator model,** *Physical Review B*, 65(9): 094412(1)- 094412(16), 2002.

جامعة النجاح الوطنية

كلية الدراسات العليا

تأثيرات المجال المغناطيسي الخارجي المنتظم ودرجة الحرارة على الخواص  
المغناطيسية لنظام ثنائي قطبي فيرومغناطيسي مضاد في بعدين: دراسة بارامترية

اعداد

نعيم" احمد رشيد" محمود ملك

اشراف

د. عبد الرحمن مصطفى ابو لبدة

قدمت هذه الأطروحة استكمالاً لمتطلبات درجة الماجستير في الفيزياء بكلية الدراسات العليا في  
جامعة النجاح الوطنية في نابلس - فلسطين.

2008

ب

تأثيرات المجال المغناطيسي الخارجي المنتظم ودرجة الحرارة على الخواص المغناطيسية  
لنظام ثنا قطبي فيرومغناطيسي مضاد في بعدين: دراسة بارامترية

اعداد

نعيم" احمد رشيد" محمود ملك

اشراف

د. عبد الرحمن مصطفى ابو لبدة

### الملخص

في هذا البحث تمت دراسة التأثيرات الناشئة عن مجال مغناطيسي خارجي منتظم على الخواص المغناطيسية لشبيكة- ثنائية البعد -مربعة- ثنا قطبية- فرومغناطيسية مضادة، لنظام ثنائي البعد بابعاد (  $104 \times 104$  ،  $64 \times 64$  ،  $32 \times 32$  )، على درجات حرارة محددة وعلى الدرجة صفر كلفن.

في هذه الدراسة، تدور العزوم المغناطيسية الكلاسيكية في مستوى النظام وتتفاعل فيما بينها من خلال تأثيرات التبادلية من نوع الفيرومغناطيسية المضادة مع الايونات المجاورة القريبة وكذلك التأثيرات الثنا قطبية ذات المدى الطويل اضافة الى المجال المغناطيسي الخارجي المنتظم الذي يؤثر على احد محوري الشبيكة.

اثناء الدراسة تم تثبيت مقدار عامل التأثيرات التبادلية  $J$  (نوع الفيرومغناطيسية المضادة) بين الايونات المتفاعلة على القيمة  $g = -1.20$  حيث تمثل  $g$  مقدار عامل التأثيرات الثنا قطبية.

بيئتُ نتائج الحسابات على درجة حرارة صفر كلفن والتي تتعلق بالمستوى الارضي للنظام، ان النظام يتحول من طور الفيرومغناطيسية الى طور الفيرومغناطيسية المضادة الثنا قطبية كلما نقصت قيمة المجال المغناطيسي الخارجي المنتظم، وان التحول يحصل على القيمة  $h_0 = 6.00$  g، وكلما نقصت قيمة شدة المجال المغناطيسي الخارجي اكثر تحدث عملية ترتيب للعزوم المغناطيسية الكلاسيكية من خلال الدوران المستمر لهذه العزوم حتى يشكل طور الفيرومغناطيسية المضادة المتعامدة مع المجال المغناطيسي الخارجي المؤثر على النظام.

ت

اظهرت النتائج ان النظام على القيمة صفر للمجال المغناطيسي المؤثر يفضل طور الفيرومغناطيسية المضادة الثنا قطبية بحيث تتم اعادة اصطفاف العزوم المغناطيسية بشكل متعامد مع المجال المغناطيسي المؤثر عليها (طور متعامد مع المجال المؤثر :  $AF_1$ ).

على درجات حرارة محدودة، تم تحديد "شكل الطور" كعلاقة بين المجال المغناطيسي الخارجي المؤثر  $h$  ودرجة الحرارة  $T$  من خلال عمليات محاكاة النظام باستخدام طريقة مونت كارلو.

على درجات حرارة منخفضة اظهرت نتائج المحاكاة ان النظام يظهر انتقالاً من الدرجة الاولى من طور الفيرومغناطيسية ( $FE$ ) الى طور الفيرومغناطيسية المضادة ( $AF$ ) كلما نقص المجال المغناطيسي المؤثر على النظام. عندما يصبح مقدار المجال المؤثر صفراً، فان النظام يفضل طور الفيرومغناطيسية المضادة الثنا قطبية بحيث تترتب العزوم المغناطيسية على زوايا  $\pm 45^\circ$  مع محور الشبكة (طور  $AF_2$ ).

على قيم صغيرة للمجال المغناطيسي الخارجي، اظهرت نتائج مونت كارلو ان النظام يظهر انتقالاً من الدرجة الثانية عندما ينتقل من طور الفيرومغناطيسية المضادة الثنا قطبية الى طور البارامغناطيسية.

على اية حال، عندما تكون قيم المجال المغناطيسي المؤثرة كبيرة جداً ودرجات الحرارة منخفضة فان النظام يترتب على طور الفيرومغناطيسية. عندما تزداد درجات الحرارة يميل النظام تدريجياً الى الفوضى ليدخل طور البارامغناطيسية.

علاوة على ذلك، اظهرت نتائج مونت كارلو في المحاكاة انه يوجد مدى من القيم للمجال المغناطيسي المؤثر يظهر فيه النظام انتقالاً من الدرجة الاولى من طور الفيرومغناطيسية المضادة الثنا قطبية الى طور الفيرومغناطيسية كلما زادت درجة الحرارة.